PROCEEDINGS A

rspa.royalsocietypublishing.org

Research

Cite this article: Schnitzer O, Giannini V, Maier SA, Craster RV. 2016 Surface plasmon resonances of arbitrarily shaped nanometallic structures in the small-screening-length limit. *Proc. R. Soc. A* **472**: 20160258.
http://dx.doi.org/10.1098/rspa.2016.0258

Received: 10 April 2016
Accepted: 3 June 2016

Subject Areas:
applied mathematics, electromagnetism, optics

Keywords:
singular perturbations, plasmonics, non-locality, surface plasmons

Author for correspondence:
Ory Schnitzer
e-mail: o.schnitzer@imperial.ac.uk

Surface plasmon resonances of arbitrarily shaped nanometallic structures in the small-screening-length limit

Ory Schnitzer[1], Vincenzo Giannini[2], Stefan A. Maier[2] and Richard V. Craster[1]

[1]Department of Mathematics, and [2]The Blackett Laboratory, Department of Physics, Imperial College London, London SW7 2AZ, UK

OS, 0000-0002-5608-2311

According to the hydrodynamic Drude model, surface plasmon resonances of metallic nanostructures blueshift owing to the non-local response of the metal's electron gas. The screening length characterizing the non-local effect is often small relative to the overall dimensions of the metallic structure, which enables us to derive a coarse-grained non-local description using matched asymptotic expansions; a perturbation theory for the blueshifts of arbitrary-shaped nanometallic structures is then developed. The effect of non-locality is not always a perturbation and we present a detailed analysis of the 'bonding' modes of a dimer of nearly touching nanowires where the leading-order eigenfrequencies and eigenmode distributions are shown to be a renormalization of those predicted assuming a local metal permittivity.

1. Introduction

Metallic nanostructures supporting localized surface plasmon resonances provide means for channelling electromagnetic energy between far and near optical fields [1]. Recent interest has focused on the ultimate limits of plasmon-assisted light confinement [2–4], particularly in the context of assemblies of metallic nanostructures separated by nanometric gaps, such as a dimer of nearly touching particles. Confinement of the electromagnetic field to dimensions comparable to those characterizing the solid-state physics leads to the breakdown of a purely classical description of the surface

THE ROYAL SOCIETY PUBLISHING

plasmon in the framework of the macroscopic Maxwell's equations with bulk values of the metal's permittivity.

A first correction, taking electron–electron interactions into account, is the non-local description of the material's polarizibility, and an implementation using the hydrodynamic Drude model [5–10] has, despite not describing the full physical reality of noble metals [11–19], led to a deeper understanding of fundamental constraints on nanoscale plasmon-assisted light localization [4,20,21]. Specifically, the case of nearly touching nanometallic structures has been studied numerically [3,22] and also via approximate analytical solutions based on transformation optics [21,23,24] and an intuitive local-analogue model [25]. At small separations, the hydrodynamic Drude model predicts that the familiar surface plasmon redshift of the 'bonding' modes with vanishing gap separation arrests at separations on the order of the Thomas–Fermi screening length. This striking prediction is consistent—up to the threshold for quantum tunnelling—with both detailed quantum-mechanical simulations [26] and experiments of light scattering from a gold sphere in near contact with a gold substrate [3].

The notion that non-locality at small scales is crucial in order to predict the surface plasmon redshift saturation for the bonding gap modes has rekindled interest in the effects of non-locality on the optical properties of isolated nanometric particles. Exact analytical solutions of the non-local hydrodynamic equations have been obtained and thoroughly analysed for spheres and circular nanowires [8,10,27], and there have also been substantial efforts to implement general codes able to overcome the challenging task of solving these equations numerically for particles of arbitrary shape [28–30]. For isolated particles, surface plasmon blueshifts predicted by the hydrodynamic Drude model are typically small (excluding tiny subnanometric particles); nevertheless, they have been observed in electron energy-loss spectroscopy experiments of nanoparticles [7]. Furthermore, they may play an important role in optical sensing and plasmon-ruler applications, especially because, contrary to quasi-static eigenfrequencies [31], non-local eigenfrequency corrections depend on size [32], in addition to shape and mode number.

We have recently put forward a novel theoretical approach for studying surface plasmon resonances [33], and effects of non-locality in particular [34], based on the paradigm of singular perturbation theory [35]. Plasmonic phenomena are often linked with physical and geometric scale disparities that can be systematically exploited to derive formulae for frequency eigenvalues and field enhancements. The approach entails scaling arguments, and the divide and conquer strategy of matched asymptotic expansions, where minimal mathematical descriptions of physically distinct regions together constitute a complete asymptotic solution of an otherwise intractable problem. This facilitates a clear physical picture of surface plasmon resonances and their near-field distributions, and in particular allows us to *a priori* identify and characterize spatial domains wherein non-locality is important and field intensity is high.

In Schnitzer *et al.* [34], we considered the plasmonic eigenvalue problem for a generic dimer system, showing via scaling and asymptotic arguments that, in the near-contact limit, non-locality acts to renormalize the otherwise singular surface plasmon redshift of the dimer's bonding modes; when the non-local screening length is small relative to particle size, the deviation of the electron density from equilibrium is exponentially confined to a narrow boundary layer adjacent to the metal–vacuum interface. The separation of scales between the boundary-layer thickness and those on which the near-field and electron-charge distributions vary along the interfaces, led to a coarse-grained local-analogue eigenvalue problem. In the resulting physical picture, the near-contact redshift saturation, or renormalization, is effectively captured by a widening of the gap.

Here we perform a detailed asymptotic analysis of the non-local hydrodynamic Drude model in the prevalent limit where the non-local screening length is small relative to the overall dimensions of the nanometallic structure. In that limit, and for smooth particles characterized by a single length scale, the local-analogue model of Schnitzer *et al.* [34] suggests that non-locality is a small perturbation. Thus, a main goal of this paper is to develop and demonstrate a perturbation theory—applicable to nanometallic structures of arbitrary shape—giving the surface plasmon blueshifts resulting from non-locality as some functional of the local-theory eigenmodes.

A second goal of this paper is to substantiate the local-analogue model of Schnitzer *et al.* [34] on the basis of the method of matched asymptotic expansions. Furthermore, we aim to clarify the justification for applying this model in the near-contact limit of a dimer structure, where the effect of non-locality is no longer a small correction, and also in excitation scenarios.

In §2, we formulate the non-local hydrodynamic Drude model, note the existence of quasi-static plasmonic eigenfrequencies and eigenmodes, and discuss several near- and far-field excitation scenarios. In §3, we revisit the analytically tractable problem of a metallic nanosphere. In §4, we carry out an *ab initio* asymptotic analysis of the surface plasmon eigenmodes of arbitrarily shaped structures characterized by a single length scale. A detailed analysis of the near-contact limit of a cylindrical dimer is carried out in §5. In §6, we relate the coarse-grained model employed in [34] with that derived in §4, and discuss its applicability more generally as a uniformly valid model, and in the context of surface plasmon excitation problems. Concluding remarks are given in §7, including a recapitulation of the key results in dimensional form.

2. Formulation

(a) Hydrodynamic Drude model

The hydrodynamic Drude model is derived in [6,10], say, and we give a brief recapitulation, assuming for simplicity that the metal is surrounded by vacuum and that metal polarization arises solely from deviations of the electron density from equilibrium. Accordingly, within the metal, Gauss's Law is

$$\epsilon_0 \boldsymbol{\nabla}\cdot\mathbf{E} = -e(n-n_{\mathrm{e}}), \tag{2.1}$$

where $\mathbf{E}$ denotes the microscopic electric field, n the electron density and n_{e} an equilibrium electron density; in vacuum (2.1) holds with the right-hand side set to zero. The electron density n and hydrodynamic velocity $\mathbf{v}$ are governed by the continuity and momentum equations

$$\frac{\partial n}{\partial t} = -\boldsymbol{\nabla}\cdot(n\mathbf{v}) \quad \text{and} \quad \left(\frac{\partial}{\partial t} + \mathbf{v}\cdot\boldsymbol{\nabla}\right)\mathbf{v} = -\frac{e}{m}(\mathbf{E}+\mathbf{v}\times\mathbf{B}) - \gamma\mathbf{v} - \beta^2\boldsymbol{\nabla}\ln n, \tag{2.2}$$

respectively. The first term on the right-hand side of the momentum equation is the Lorentz force ($\mathbf{B}$ being the magnetic induction and m the effective electron mass), the second is a phenomenological dissipation term (γ is a collision frequency) and the third is an electron-pressure term derived from the Thomas–Fermi energy functional; the parameter β is a non-locality parameter, that, for frequencies $\omega \gg \gamma$, is $\beta^2 = 3v_{\mathrm{F}}^2/5$, v_{F} being the Fermi velocity. Assuming that the electrons are confined to the metal domain, the metal–vacuum interfacial conditions read

$$[\hat{\mathbf{n}}\cdot\mathbf{E}] = 0, \quad [\hat{\mathbf{n}}\times\mathbf{E}] = 0 \quad \text{and} \quad \hat{\mathbf{n}}\cdot\mathbf{v} = 0, \tag{2.3}$$

where $\hat{\mathbf{n}}$ denotes an outward unit normal and square brackets the difference across the interface.

We follow the standard procedure of linearization assuming a small, time harmonic, deviation of electron density from equilibrium: $n - n_{\mathrm{e}} \approx \mathrm{Re}[\mathrm{e}^{-\mathrm{i}\omega t}n']$, and similarly $\mathbf{E} \approx \mathrm{Re}[\mathrm{e}^{-\mathrm{i}\omega t}\mathbf{E}']$, $\mathbf{B} \approx \mathrm{Re}[\mathrm{e}^{-\mathrm{i}\omega t}\mathbf{B}']$ and $\mathbf{v} \approx \mathrm{Re}[\mathrm{e}^{-\mathrm{i}\omega t}\mathbf{v}']$. Equations (2.1)–(2.2) governing the metal domain become

$$\epsilon_0\boldsymbol{\nabla}\cdot\mathbf{E}' = -en' \tag{2.4}$$

and

$$\mathrm{i}\omega n' = n_{\mathrm{e}}\boldsymbol{\nabla}\cdot\mathbf{v}', \quad (-\mathrm{i}\omega+\gamma)\mathbf{v}' = -\frac{e}{m}\mathbf{E}' - \frac{\beta^2}{n_{\mathrm{e}}}\boldsymbol{\nabla}n'. \tag{2.5}$$

Linearizing the interfacial conditions (2.3) gives

$$[\hat{\mathbf{n}}\cdot\mathbf{E}'] = 0, \quad [\hat{\mathbf{n}}\times\mathbf{E}'] = 0 \quad \text{and} \quad \hat{\mathbf{n}}\cdot\left(\mathbf{E}' + \frac{m\beta^2}{en_{\mathrm{e}}}\boldsymbol{\nabla}n'\right) = 0. \tag{2.6}$$

Eliminating $\mathbf{v}'$ from the formulation by combining (2.5) gives the scalar equation

$$\frac{\beta^2}{\omega_\mathrm{p}^2}\nabla^2 n' = \left(1 - \frac{\omega^2 + \mathrm{i}\gamma\omega}{\omega_\mathrm{p}^2}\right) n', \tag{2.7}$$

where $\omega_\mathrm{p} = e\sqrt{n_\mathrm{e}/\epsilon_\mathrm{e} m}$ is the metal's plasma frequency. The subnanometric length scale $\lambda_\mathrm{F} = \beta/\omega_\mathrm{p}$, roughly 0.2 nm for gold, characterizes electron-density variations in the metal; we shall refer to it as the non-local screening length. In terms of the 'local' Drude dielectric function [1],

$$\epsilon = 1 - \frac{\omega_\mathrm{p}^2}{\omega^2 + \mathrm{i}\gamma\omega}, \tag{2.8}$$

Equation (2.7) equivalently reads as

$$\lambda_\mathrm{F}^2 \nabla^2 n' = \frac{\epsilon}{\epsilon - 1} n'. \tag{2.9}$$

In principal, we must supplement Guass's Law (2.4) by the remaining Maxwell equations. At this stage, however, we invoke the quasi-static approximation [1], appropriate for deeply subwavelength plasmonic structures of characteristic size $\ll c/(\omega\sqrt{|\epsilon|})$, c being the speed of light in vacuum. The electric near field is then irrotational, $\boldsymbol{\nabla} \times \mathbf{E}' \approx 0$, allowing us to introduce an electric potential φ' such that $\mathbf{E}' = -\boldsymbol{\nabla}\varphi'$.

(b) Surface plasmons and their excitation

Our formulation governing the near field of the nanometric particle is closed by conditions at (subwavelength) distances large relative to its dimensions, which depend on the specific scenario under consideration, and, in general, arise through a matching procedure with the optical far field. For example, to a first approximation, illumination by an electromagnetic plane wave is experienced by a deeply subwavelength particle as an incident uniform time-harmonic electric field. The relevant condition is then $\mathbf{E}' \sim \hat{\boldsymbol{\imath}} E_\infty$ as $|\boldsymbol{X}| \to \infty$, where E_∞ and $\hat{\boldsymbol{\imath}}$ are the magnitude and polarization of the incident field, respectively, and $\boldsymbol{X}$ is a position vector relative to some point within the particle. From the properties of Laplace's equation we then have [36]

$$\varphi' \sim -E_\infty \hat{\boldsymbol{\imath}} \cdot \boldsymbol{X} + \frac{\boldsymbol{p} \cdot \boldsymbol{X}}{4\pi\epsilon_0 |\boldsymbol{X}|^3} + \cdots \quad \text{as } |\boldsymbol{X}| \to \infty, \tag{2.10}$$

where the polarization vector $\boldsymbol{p}$ is an outcome of the near-field problem, from which quasi-static approximations for the far-field optical cross sections can be derived [1]. In particular, the absorption cross section in the direction of $\hat{\boldsymbol{\imath}}$ is

$$\mathcal{C}_\mathrm{abs} = \frac{\omega}{c\epsilon_0 E_\infty} \mathrm{Im}(\boldsymbol{p} \cdot \hat{\boldsymbol{\imath}}). \tag{2.11}$$

If, instead of incident radiation, the forcing is in the near field then the vacuum potential φ' attenuates at large distances. In §3, we consider one such example where the forcing is due to a radiating molecule in the vicinity of a nanometallic particle. A radiating molecule is often modelled as an oscillating electric-dipole singularity, with position vector $\boldsymbol{X}_J$; hence, in this case the Laplace equation governing the vacuum potential φ' is replaced by

$$\mathrm{i}\omega\epsilon_0 \nabla^2 \varphi' = -\boldsymbol{J}' \cdot \boldsymbol{\nabla}\delta_\mathrm{D}(\boldsymbol{X} - \boldsymbol{X}_J), \tag{2.12}$$

where $\boldsymbol{J} = \mathrm{Re}[\mathrm{e}^{-\mathrm{i}\omega t}\boldsymbol{J}']$ is the current-density vector and δ_D denotes the Dirac delta function.

In the present context, the phenomenon of plasmon resonance crucially relies on the existence, in the absence of external forcing and dissipation ($\gamma = 0$), of non-trivial solutions that attenuate at large distances; this defines a plasmonic eigenvalue problem and we refer to the eigensolutions as the plasmon modes of the metallic nanoparticle. More specifically, for $\omega < \omega_\mathrm{p}$, (2.7) is a modified Helmholtz equation, and eigensolutions are called 'surface plasmons' since these exhibit an electron-charge distribution confined to a narrow layer adjacent to the surface of the particle. For $\omega > \omega_\mathrm{p}$, (2.7) is a proper Helmholtz equation, and eigensolutions are called 'bulk plasmons'; these

exhibit a spatially oscillating electron-density distribution. Modes of the latter type are entirely missed when working in a local formulation where electron-density polarization is effectively accounted for in terms of a macroscopic dielectric function.

The physical significance of plasmon eigenmodes stems from the smallness of γ, for certain plasmonic metals such as gold and silver, relative to typical surface plasmon eigenfrequencies. Thence, under an external forcing, close to a plasmon eigenfrequency, and having correct symmetries, a damped resonance occurs. That is, to leading order (in γ/ω) the near-field distribution mimics that of the corresponding eigenmode, with a large amplitude factor relative to the externally applied field.

(c) Dimensionless formulation

It is convenient to adopt a dimensionless formulation where lengths are normalized by a characteristic dimension a, and potentials by aE, E being a reference field-magnitude value. Specifically, we define the dimensionless position vector $\mathbf{x} = \boldsymbol{X}/a$, potential $\varphi = \varphi'/(aE)$ and the dimensionless screening length $\delta = \lambda_{\mathrm{F}}/a$. From Gauss's Law (2.4), we obtain $n' = O(\epsilon_0 E/e\lambda_{\mathrm{F}})$, suggesting a dimensionless charge density $q = -e\lambda_{\mathrm{F}} n'/(\epsilon_0 E)$. Equations (2.4) and (2.7) governing the metal domain become

$$\delta^2\nabla^2 q = \frac{\epsilon}{\epsilon - 1} q \quad \text{and} \quad \delta\nabla^2\varphi = -q, \tag{2.13}$$

where ϵ denotes the local Drude function (2.8). In vacuum, q is zero and φ is governed by the Laplace equation. The interfacial conditions (2.6) become

$$[\varphi] = 0, \quad \left[\frac{\partial\varphi}{\partial n}\right] = 0, \quad \frac{\partial\varphi}{\partial n} + \delta\frac{\partial q}{\partial n} = 0. \tag{2.14}$$

Occasionally, it is convenient to use a formulation wherein within the metal we solve for $\chi = \varphi + \delta q$, instead of φ, and solve Laplace's equation for φ in vacuum, and (2.13), rewritten as

$$\delta^2\nabla^2 q = \frac{\epsilon}{\epsilon - 1} q \quad \text{and} \quad \delta\nabla^2\chi = \frac{1}{\epsilon - 1} q, \tag{2.15}$$

in the metal domain. The interfacial conditions (2.14) are rewritten as

$$\varphi = \chi - \delta q, \quad \frac{\partial\chi}{\partial n} = 0 \quad \text{and} \quad \frac{\partial\varphi}{\partial n} + \delta\frac{\partial q}{\partial n} = 0. \tag{2.16}$$

3. Metallic nanosphere

It is instructive to begin by reviewing the case of a spherical metallic particle, which is amenable to an 'exact' analytical analysis [8,10,27,37]. Emphasis will be placed on approximate simplifications in certain limits, with the intention of motivating the asymptotic approach adopted in later sections. Considering the scenario of plane-wave illumination as discussed in §§2b, the dimensionless equations of §§2c are supplemented by the far-field condition

$$\varphi \sim -\hat{\boldsymbol{\imath}} \cdot \mathbf{x} + o(1) \quad \text{as } |\mathbf{x}| \to \infty, \tag{3.1}$$

where the reference length scale a and field magnitude E have been chosen, respectively, as the sphere radius and incident field E_∞. Separation of variables provides the deviation of the vacuum potential from the uniform applied field as (cf. (2.10))

$$\varphi + \hat{\boldsymbol{\imath}} \cdot \mathbf{x} = \mu \frac{\hat{\boldsymbol{\imath}} \cdot \mathbf{x}}{|\mathbf{x}|^3}, \quad \text{wherein } \mu = \frac{(\epsilon - 1)[\mathrm{i}k j_1'(\mathrm{i}k) - j_1(\mathrm{i}k)]}{\mathrm{i}k(\epsilon + 2) j_1'(\mathrm{i}k) + 2(\epsilon - 1) j_1(\mathrm{i}k)} \tag{3.2}$$

is the dimensionless induced-dipole moment $\boldsymbol{p} \cdot \hat{\boldsymbol{\imath}}/(4\pi\epsilon_0 a^3 E)$. In (3.2), j_1 is the spherical Bessel function of the first kind, and $k(\delta, \epsilon)$ is defined through

$$\delta^2 k^2(\epsilon - 1) = \epsilon, \tag{3.3}$$

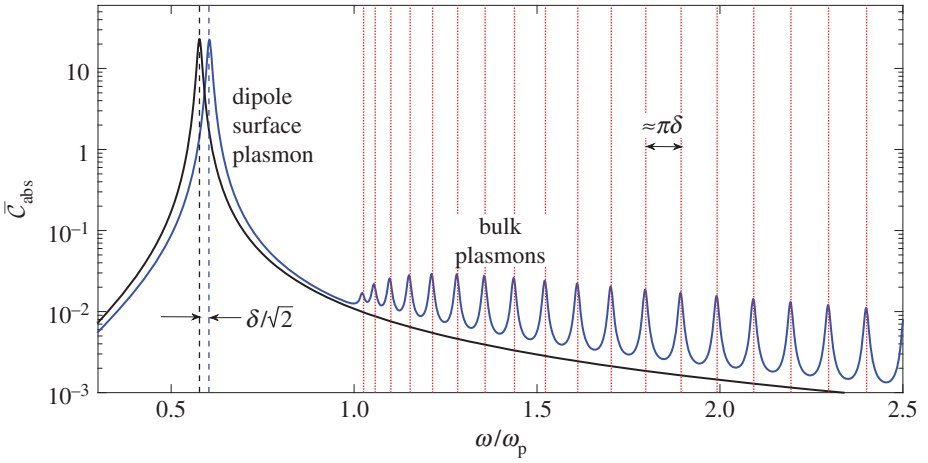

Figure 1. Normalized absorption cross-section (3.4) for a metal nanosphere (using typical values $a = 2$ nm, $\beta = 10^6$ m s^{-1}, $\hbar\omega_{\rm p} = 9$ eV and $\hbar\gamma = 0.13$ eV [25,27]) with $\delta \approx 0.037$ under plane-wave illumination. Black line, local prediction [1]; blue line, non-local prediction (3.2); dashed black and blue lines, local and non-local predictions of resonant frequency, respectively (cf. (3.7)) and dotted red lines, (3.8) for the high-order bulk-plasmon frequencies. (Online version in colour.)

with $k > 0$ for $\epsilon < 0$. In figure 1, for typical parameters used in the literature, we plot the normalized absorption cross-section $\bar{C}_{\rm abs} = C_{\rm abs}/[4\pi a^3(\omega_{\rm p}/c)]$, or

$$\bar{C}_{\rm abs} = \frac{\omega}{\omega_{\rm p}}{\rm Im}[\mu], \tag{3.4}$$

with μ given by (3.2), and by its 'local' counterpart [1]

$$\mu = \frac{\epsilon - 1}{\epsilon + 2}. \tag{3.5}$$

For $\omega < \omega_{\rm p}$, plane-wave illumination excites only the fundamental 'dipolar' surface plasmon mode of the sphere, which is notably blueshifted from the local-theory prediction represented by the 'Frohlich condition': ${\rm Re}[\epsilon] = -2$. Notably, there are also multiple weak bulk-plasmon modes excited for $\omega > \omega_{\rm p}$, a feature not captured by a local model.

From (3.2), the resonance frequencies of the excited plasmon modes are governed by the transcendental equation

$${\rm i}k(\epsilon + 2)j_1'({\rm i}k) + 2(\epsilon - 1)j_1({\rm i}k) = 0, \tag{3.6}$$

which in general needs to be solved numerically. The typical smallness of the dimensionless screening length δ, which is embedded in k, suggests, however, seeking asymptotic solutions. In fact, the surface plasmon solution of (3.6) in the limit $\delta \ll 1$ is readily found as $\epsilon \sim -2 + 6\delta\sqrt{3/2} + O(\delta^2)$, where the leading-order term agrees with the local-theory prediction. Recalling (2.8), the corresponding resonance frequency is

$$\frac{\omega}{\omega_{\rm p}} \sim \frac{1}{\sqrt{3}} + \delta\frac{1}{\sqrt{2}} + O(\delta^2). \tag{3.7}$$

The blueshift predicted by (3.7) is depicted in figure 1 by dashed vertical lines. As in previous studies [10], we derived (3.7) by reducing the closed-form solution for a sphere in the limit $\delta \to 0$. As we shall see in §4, it is also possible to alternatively derive (3.7) by a direct asymptotic analysis of the non-local equations. In fact, one of our main goals is to obtain analogous blueshift formulae for arbitrarily shaped particles for which closed-form solutions do not exist.

Asymptotic analysis of (3.6) in the limit $\delta \to 0$ also provides the bulk-plasmon frequencies as solutions of the transcendental equation ${\rm i}k\tan({\rm i}k) \sim 2(\epsilon - 1)/(\epsilon + 2)$. Together with (2.8), an

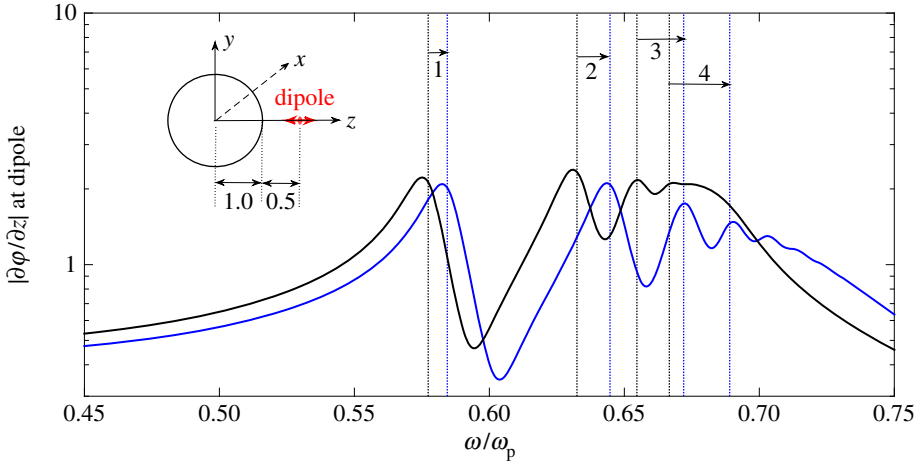

Figure 2. Multimode excitation of a metal sphere by a nearby radially oriented electric dipole positioned as shown in the inset ($\hbar\omega_p = 9$ eV, $\hbar\gamma = 0.13$ eV and $\delta = 0.01$). Black and blue lines, absolute magnitude of the induced radial field at the position of the dipole according to the local and non-local models, respectively. Vertical black and blue dotted lines, first and first two terms of (3.10). (Online version in colour.)

explicit high-mode-number approximation for the bulk-plasmon frequencies is found as

$$\frac{\omega}{\omega_p} \sim (1 + n^2\pi^2\delta^2)^{1/2}, \quad n \text{ integer } \gg 1. \tag{3.8}$$

The predictions of (3.8) are depicted by the dotted red lines in figure 1; they accurately pinpoint the resonance peaks, starting from nearly the first bulk resonance. When $n \gg 1/\delta$, $\omega/\omega_p \approx n\pi\delta$, and hence the bulk plasmon frequencies become uniformly separated by $\approx \pi\delta$. As far as we are aware, formula (3.8) for the bulk modes of a sphere is new.

For the highly symmetric scenario of plane-wave illumination of a sphere particle, only the dipolar, or Fröhlich, surface plasmon mode is excited. It is important to emphasize, however, that a nanometallic sphere actually supports an infinite number of surface plasmons. To demonstrate this we consider a less symmetric forcing in the form of a radiating molecule, modelled as a radially oriented electric dipole placed half a radius away from the particle boundary, with $\boldsymbol{J}' = \mathcal{J}\hat{\boldsymbol{\imath}}$ in (2.12). With a reference field value $E = \mathcal{J}/(\epsilon_0\omega_p)$, and defining a dimensionless cartesian system (x, y, z) as shown in figure 2, with $\hat{\mathbf{e}}_z = \hat{\boldsymbol{\imath}}$, (2.12) governing the vacuum potential becomes

$$\nabla^2\varphi = \mathrm{i}\frac{\omega_p}{\omega}\hat{\mathbf{e}}_z \cdot \boldsymbol{\nabla}[\delta_D(x)\delta_D(y)\delta_D(z - l)], \tag{3.9}$$

with φ attenuating at large distances. While more tedious, separation of variables can here too be applied once the singularity on the right-hand side of (3.9) is expanded in spherical harmonics. Of interest is the field induced at the location of the dipole, from which a decay rate can be calculated [8,27]. In figure 2, we show the dimensionless radial field there, blue line, along with the local-theory prediction, black line. In contrast with the plane-wave case, several peaks are seen for $\omega < \omega_p$. While the surface plasmon frequencies can be extracted from the analytic solution (as in e.g. Ref. [10]), we exploit the general theory for arbitrarily shaped particles to be developed in §4, which in particular yields the surface plasmon frequencies of a sphere as

$$\frac{\omega}{\omega_p} \sim \sqrt{\frac{l}{2l+1}} + \frac{1}{2}\delta\sqrt{l(l+1)} + O(\delta^2), \quad l = 1, 2, \ldots . \tag{3.10}$$

The above equation agrees with expressions in the literature based on reductions of analytical solutions [7,8,10]. Note that (3.7) is a special case of (3.10) for $l = 1$. The applicability of (3.10) is demonstrated in figure 2, where the first, and then both (local and then non-local) terms of (3.10)

are depicted by the vertical dashed black and blue lines, respectively. Notably the effect of non-locality is stronger for higher-order modes, suggesting the effect is easier to observe under near-field excitation [8]. An intuitive explanation is that the relative impact of non-locality depends on the ratio between the screening length λ_F and the characteristic length scale characterizing a mode. For low-order modes, the latter can be taken to be a, here the sphere radius. Higher modes vary more rapidly, and a suitable characteristic scale is a/l. This explains the $O(\delta l)$ and $O(\delta n)$ effect in (3.10) and (3.8), respectively. Specifically, (3.10) is no longer asymptotic for $l \gg 1/\delta$; such high-order surface plasmons can be excited by electron beams [38], but not with light. The above discussion hints that non-locality could play a crucial role when a characteristic scale of the geometry is comparable to λ_F, a scenario we shall return to in §4f and §4g and consider in detail in §5.

4. Plasmon blueshift of arbitrarily shaped particles

(a) The small-screening-length limit

Henceforth, our interest is in a direct asymptotic analysis of the non-local hydrodynamic equations in the limit $\delta \to 0$ with the obvious expectation that, to leading order, the local electromagnetic approximation is recovered. This requires choosing the length scale a to be the smallest one characterizing all relevant modes, and, in this section, we enforce this by focusing on low-order surface plasmon modes of metallic nanostructures with a single geometric length scale $a \gg \lambda_F$. An intuitive way to 'derive' the local approximation from the non-local equations is to set $\beta = 0$ in (2.5), which together with (2.4) immediately leads to a local relation between electric displacement and field involving the Drude dielectric function (2.8), and demanding normal-displacement and tangential-field continuity at the metal–vacuum interface. Such arguments, however, are heuristic, and do not suggest how to systematically go beyond the local approximation.

The results of §3 imply that non-locality manifests itself as a surface plasmon blueshift relative to the resonant frequencies of the local approximation. Motivated by this, we now consider the surface plasmon eigenvalue problem for an arbitrary single-scale particle and ask for what discrete and real frequencies below ω_p (alternatively, real and negative ϵ values) does a solution of the non-local equations exist with the vacuum potential attenuating at large distances. Following the results of §3, we anticipate an eigenvalue expansion in the form

$$\epsilon \sim \epsilon^{(0)} + \delta\epsilon^{(1)} + \cdots, \tag{4.1}$$

the corresponding resonance-frequency expansion following from (2.8) as

$$\frac{\omega}{\omega_p} \sim (1-\epsilon^{(0)})^{-1/2} + \frac{1}{2}\delta\epsilon^{(1)}(1-\epsilon^{(0)})^{-3/2} + \cdots. \tag{4.2}$$

Naively, the regular expansion (4.1) suggests a comparable expansion of the eigenpotential and charge density. Assuming without loss of generality that the former is $O(1)$, and letting $\bar{\varphi}$ represent the metal-domain potential, we write

$$\varphi \sim \varphi^{(0)}(\mathbf{x}) + \delta\varphi^{(1)}(\mathbf{x}) + \cdots \quad \text{and} \quad \bar{\varphi} \sim \bar{\varphi}^{(0)}(\mathbf{x}) + \delta\bar{\varphi}^{(1)}(\mathbf{x}) + \cdots. \tag{4.3}$$

For $\epsilon < 0$, it is readily seen from (2.13) that a regular expansion for q would vanish at every algebraic order in δ. On one hand, this implies that q is exponentially small, whereby from (2.13)

$$\nabla^2\varphi^{(m)}(\mathbf{x}) = 0 \quad \text{and} \quad \nabla^2\bar{\varphi}^{(m)}(\mathbf{x}) = 0, \tag{4.4}$$

for all orders $m = 0, 1, 2, \ldots$. On the other hand, the interfacial conditions (2.14) demand $\partial q/\partial n = O(1/\delta)$. The regular expansion for $\bar{\varphi}$ in (4.3) must therefore break down at $O(\delta)$ distances from the interface, where (2.13) implies an exponential attenuation of an $q = O(1)$ charge density and consequently a rapid inharmonic variation of $\bar{\varphi}$.

The limit $\delta \to 0$ is spatially non-uniform and must accordingly be addressed using singular perturbation theory and we employ matched asymptotic expansions to conceptually decompose the metal domain into two regions: (i) an electron-charge boundary layer of width $O(\delta)$ adjacent to the metal–vacuum interface, where $q = O(1)$ and $\bar{\varphi}$ is inharmonic; and (ii) a bulk-metal domain where $\mathbf{x} = O(1)$, q is exponentially small and $\bar{\varphi}$ is harmonic to all orders. The plan is to locally analyse the boundary layer and thereby derive effective boundary conditions connecting the metal and vacuum bulk domains at successive orders in δ.

(b) Boundary-layer analysis

We take an arbitrary smooth particle and grid its boundary by orthogonal unit-metric surface coordinates (ξ, η) with unit vectors $(\hat{\mathbf{e}}_\xi, \hat{\mathbf{e}}_\eta)$. At a surface point $\mathscr{P} = (\xi, \eta)$, we define a cartesian coordinate system (x, y, z) with origin at $\mathscr{P}$ and unit vectors $(\hat{\mathbf{e}}_x, \hat{\mathbf{e}}_y, \hat{\mathbf{e}}_z)$, where $\hat{\mathbf{e}}_x, \hat{\mathbf{e}}_y$ are locally parallel to $\hat{\mathbf{e}}_\xi, \hat{\mathbf{e}}_\eta$, and $\hat{\mathbf{e}}_z$ points in the direction of the local outward normal $\hat{\mathbf{n}}$. We also define a stretched boundary-layer coordinate $Z = z/\delta$. The boundary-layer fields can be written as

$$q = Q(\xi, \eta, Z) \quad \text{and} \quad \chi = \varphi^{(0)}(\xi, \eta) + \delta T(\xi, \eta, Z), \tag{4.5}$$

where bulk fields appearing in boundary-layer equations, e.g. $\varphi^{(0)}$ in (4.5), are understood to correspond to limiting values as the interface is approached, and are accordingly functions of (ξ, η) alone. (In the boundary layer, it is convenient to work with χ rather than $\bar{\varphi}$; note that in the metal bulk these two are the same to exponential order.) A non-trivial subtlety is that Q and T are sought as functions of Z and (ξ, η), rather than Z and (x, y). Thus in what follows partial derivatives with respect to Z are with (ξ, η), rather than (x, y), held constant. This approach will allow us to conveniently apply boundary conditions at $Z = 0$ rather than on a curved surface (for further discussion, see e.g. [39]).

Noting that $\nabla^2 \chi = \nabla_s^2 \varphi^{(0)} + \delta \nabla^2 T$, where ∇_s^2 is the surface Laplacian, (2.15) become

$$\delta(\boldsymbol{\nabla} \cdot \hat{\mathbf{n}}) \frac{\partial Q}{\partial Z} + \frac{\partial^2 Q}{\partial Z^2} = \frac{\epsilon}{\epsilon - 1} Q + O(Q\delta^2) \tag{4.6}$$

and

$$\delta \left(\nabla_s^2 \varphi^{(0)} + \boldsymbol{\nabla} \cdot \hat{\mathbf{n}} \frac{\partial T}{\partial Z} \right) + \frac{\partial^2 T}{\partial Z^2} = \frac{1}{\epsilon - 1} Q + O(T\delta^2), \tag{4.7}$$

where the unspecified correction terms correspond to higher order terms in the coordinate transformation. The interfacial conditions (2.16) read

$$\frac{\partial Q}{\partial Z} = -\frac{\partial \varphi}{\partial n}, \quad \frac{\partial T}{\partial Z} = 0 \quad \text{and} \quad \varphi - \varphi^{(0)} = \delta(T - Q) \quad \text{at } Z = 0. \tag{4.8}$$

Additional conditions are derived by matching the boundary-layer fields with their metal-bulk counterparts. The matching conditions on Q are attenuation at every algebraic order, as q is exponentially small in the bulk. Those on T are inferred from the Taylor expansion of the bulk potential $\bar{\varphi}$ in the vicinity of $\mathscr{P}$, rewritten in terms of Z. The resulting matching condition reads as

$$\begin{aligned} \chi \sim{}& \bar{\varphi}^{(0)} + \delta \left(Z \frac{\partial \bar{\varphi}^{(0)}}{\partial n} + \bar{\varphi}^{(1)} \right) \\ &+ \delta^2 \left[-\frac{1}{2} Z^2 \left(\boldsymbol{\nabla} \cdot \hat{\mathbf{n}} \frac{\partial \bar{\varphi}^{(0)}}{\partial n} + \nabla_s^2 \bar{\varphi}^{(0)} \right) + Z \frac{\partial \bar{\varphi}^{(1)}}{\partial n} + \bar{\varphi}^{(2)} \right] + \cdots \quad \text{as } Z \to -\infty. \end{aligned} \tag{4.9}$$

We now expand the boundary-layer fields in the form

$$Q \sim Q^{(0)} + \delta Q^{(1)} + \cdots \quad \text{and} \quad T \sim T^{(1)} + \delta T^{(2)} + \cdots. \tag{4.10}$$

Substituting (4.10) into (4.6) we find at leading order the governing equations

$$\frac{\partial^2 T^{(1)}}{\partial Z^2} = \frac{1}{\epsilon^{(0)} - 1} Q^{(0)} \quad \text{and} \quad \frac{\partial^2 Q^{(0)}}{\partial Z^2} = \frac{\epsilon^{(0)}}{\epsilon^{(0)} - 1} Q^{(0)} \tag{4.11}$$

and at first order

$$\frac{\partial^2 T^{(2)}}{\partial Z^2} = \frac{1}{\epsilon^{(0)}-1} Q^{(1)} - \frac{\epsilon^{(1)}}{(\epsilon^{(0)}-1)^2} Q^{(0)} - \nabla_s^2 \varphi^{(0)} - \boldsymbol{\nabla}\cdot\hat{\mathbf{n}} \frac{\partial T^{(1)}}{\partial Z} \tag{4.12}$$

and

$$\frac{\partial^2 Q^{(1)}}{\partial Z^2} - \frac{\epsilon^{(0)}}{\epsilon^{(0)}-1} Q^{(1)} = -\frac{\epsilon^{(1)}}{(\epsilon^{(0)}-1)^2} Q^{(0)} - (\boldsymbol{\nabla}\cdot\hat{\mathbf{n}}) \frac{\partial Q^{(0)}}{\partial Z}. \tag{4.13}$$

Equations (4.11)–(4.13) are supplemented by the interfacial conditions (cf. (4.8))

$$\frac{\partial Q^{(0)}}{\partial Z} = -\frac{\partial \varphi^{(0)}}{\partial n}, \quad \frac{\partial Q^{(1)}}{\partial Z} = -\frac{\partial \varphi^{(1)}}{\partial n}, \quad \frac{\partial T^{(1)}}{\partial Z} = \frac{\partial T^{(2)}}{\partial Z} = 0 \tag{4.14}$$

and

$$\varphi^{(1)} = T^{(1)} - Q^{(0)} \quad \text{at } Z = 0 \tag{4.15}$$

and the matching conditions (cf. (4.9))

$$\bar{\varphi}^{(0)} = \varphi^{(0)} \quad \text{as} \quad Z \to -\infty, \tag{4.16}$$

$$T^{(1)} \sim Z \frac{\partial \bar{\varphi}^{(0)}}{\partial n} + \bar{\varphi}^{(1)} \quad \text{as} \quad Z \to -\infty \tag{4.17}$$

and

$$T^{(2)} \sim -\frac{1}{2} Z^2 \left(\boldsymbol{\nabla}\cdot\hat{\mathbf{n}} \frac{\partial \bar{\varphi}^{(0)}}{\partial n} + \nabla_s^2 \bar{\varphi}^{(0)} \right) + Z \frac{\partial \bar{\varphi}^{(1)}}{\partial n} + \bar{\varphi}^{(2)} \quad \text{as } Z \to -\infty. \tag{4.18}$$

Note in particular that (4.16) serves as our first effective interfacial condition. As already noted, matching also entails

$$Q^{(0)}, Q^{(1)}, Q^{(2)}, \ldots \to 0 \quad \text{as } Z \to -\infty. \tag{4.19}$$

Solving (4.11) in conjunction with (4.14) and (4.19) gives

$$Q^{(0)} = -\left(\frac{\epsilon^{(0)}-1}{\epsilon^{(0)}} \right)^{1/2} \frac{\partial \varphi^{(0)}}{\partial n} \exp\left[\left(\frac{\epsilon^{(0)}}{\epsilon^{(0)}-1} \right)^{1/2} Z \right] \tag{4.20}$$

and

$$T^{(1)} = -\left(\frac{\epsilon^{(0)}-1}{\epsilon^{(0)}} \right)^{1/2} \frac{1}{\epsilon^{(0)}} \frac{\partial \varphi^{(0)}}{\partial n} \exp\left[\left(\frac{\epsilon^{(0)}}{\epsilon^{(0)}-1} \right)^{1/2} Z \right] + \frac{1}{\epsilon^{(0)}} \frac{\partial \varphi^{(0)}}{\partial n} Z + \bar{\varphi}^{(1)}. \tag{4.21}$$

Comparing (4.21) with the matching condition (4.17) yields a second effective interfacial condition

$$\frac{\partial \varphi^{(0)}}{\partial n} = \epsilon^{(0)} \frac{\partial \bar{\varphi}^{(0)}}{\partial n}. \tag{4.22}$$

As anticipated, the two leading-order effective conditions (4.16) and (4.22) are nothing but the familiar 'local' boundary conditions. To go beyond the local approximation, we require two effective interfacial conditions at $O(\delta)$. The first of these,

$$\varphi^{(1)} - \bar{\varphi}^{(1)} = \left(\frac{\epsilon^{(0)}-1}{\epsilon^{(0)}} \right)^{3/2} \frac{\partial \varphi^{(0)}}{\partial n}, \tag{4.23}$$

follows from potential continuity (4.15). Towards deriving the second, we integrate (4.12) with respect to Z, whereby together with (4.19) and (4.21) we find

$$\begin{aligned} \frac{\partial T^{(2)}}{\partial Z} \sim & -Z \left(\boldsymbol{\nabla}_s^2 \varphi^{(0)} + \frac{1}{\epsilon^{(0)}} \frac{\partial \varphi^{(0)}}{\partial n} \boldsymbol{\nabla}\cdot\hat{\mathbf{n}} \right) - \frac{1}{\epsilon^{(0)}-1} \int_{-\infty}^{0} Q^{(1)} \, \mathrm{d}Z \\ & + \frac{\epsilon^{(1)}}{(\epsilon^{(0)}-1)^2} \int_{-\infty}^{0} Q^{(0)} \, \mathrm{d}Z - \boldsymbol{\nabla}\cdot\hat{\mathbf{n}} \left(\frac{\epsilon^{(0)}-1}{\epsilon^{(0)}} \right)^{1/2} \frac{1}{\epsilon^{(0)}} \frac{\partial \varphi^{(0)}}{\partial n} + o(1) \quad \text{as } Z \to -\infty. \end{aligned} \tag{4.24}$$

In (4.24), the integral of $Q^{(0)}$ is calculated using (4.20), whereas the integral of $Q^{(1)}$ is obtained by integrating (4.13) with respect to Z together with (4.19) and (4.14). Equation (4.24) then gives

$$\frac{\partial T^{(2)}}{\partial Z} \sim -Z\left(\boldsymbol{\nabla}_s^2\varphi^{(0)} + \frac{1}{\epsilon^{(0)}}\frac{\partial\varphi^{(0)}}{\partial n}\boldsymbol{\nabla}\cdot\hat{\mathbf{n}}\right) + \frac{1}{\epsilon^{(0)}}\frac{\partial\varphi^{(1)}}{\partial n} - \frac{\epsilon^{(1)}}{\epsilon^{(0)}}\frac{\partial\varphi^{(0)}}{\partial n} + o(1) \quad \text{as } Z\to-\infty. \tag{4.25}$$

Comparing with (4.18), we find that the term $\propto Z$ identically matches, whereas matching the $O(1)$ term furnishes the second $O(\delta)$ effective condition as

$$\frac{\partial\varphi^{(1)}}{\partial n} - \epsilon^{(0)}\frac{\partial\bar{\varphi}^{(1)}}{\partial n} = \frac{\epsilon^{(1)}}{\epsilon^{(0)}}\frac{\partial\varphi^{(0)}}{\partial n}. \tag{4.26}$$

(c) Coarse-grained eigenvalue problem

To summarize the coarse-grained eigenvalue problem, the bulk potentials $\bar{\varphi}$ and φ, expanded as in (4.3), are governed by Laplace's equation at each order, attenuate at large distances, and satisfy effective interfacial conditions applying at an effective interface, which geometrically coincides with the true vacuum–metal interface. At leading order these conditions are (cf. (4.16) and (4.22))

$$\varphi^{(0)} = \bar{\varphi}^{(0)} \quad \text{and} \quad \frac{\partial\varphi^{(0)}}{\partial n} = \epsilon^{(0)}\frac{\partial\bar{\varphi}^{(0)}}{\partial n}, \tag{4.27}$$

which, together with attenuation of $\varphi^{(0)}$, define the 'local' plasmonic eigenvalue problem governing the leading eigenvalues $\epsilon^{(0)}$ and eigenpotentials $(\varphi^{(0)},\bar{\varphi}^{(0)})$. At $O(\delta)$, the effective conditions are (cf. (4.23) and (4.26))

$$\varphi^{(1)} - \bar{\varphi}^{(1)} = \left(\frac{\epsilon^{(0)}-1}{\epsilon^{(0)}}\right)^{3/2}\frac{\partial\varphi^{(0)}}{\partial n} \quad \text{and} \quad \frac{\partial\varphi^{(1)}}{\partial n} - \epsilon^{(0)}\frac{\partial\bar{\varphi}^{(1)}}{\partial n} = \epsilon^{(1)}\frac{\partial\bar{\varphi}^{(0)}}{\partial n}. \tag{4.28}$$

Together with attenuation of $\varphi^{(1)}$, (4.28) define a correction problem governing the perturbations $\epsilon^{(1)}$ and $(\varphi^{(1)},\bar{\varphi}^{(1)})$. Equation (4.28) shows that, to $O(\delta)$, non-locality manifests itself macroscopically as an effective potential discontinuity; the local displacement-continuity condition remains valid to this order. Determining the eigenvalue correction $\epsilon^{(1)}$ does not require a detailed solution of the $O(\delta)$ problem. Rather, as we show next, $\epsilon^{(1)}$ can be obtained directly from knowledge of the 'local' eigenvalues and eigenpotentials. In essence, our coarse-graining procedure has regularized the otherwise singular small-δ limit, allowing us to apply standard ideas of regular perturbation theory.

(d) Non-local perturbation from simple and degenerate eigenvalues

We first take $\epsilon^{(0)}$ as a simple eigenvalue linked with one distinct eigenpotential pair $(\varphi^{(0)},\bar{\varphi}^{(0)})$. Since attenuation at large distances and Laplace's equation hold at each algebraic order, the correction problem (cf. (4.28)) is a forced version of the leading-order local problem (cf. (4.27)). The former can, therefore, posses a solution only under special circumstances. Indeed, applying Green's second identity to the pairs $(\varphi^{(0)},\varphi^{(1)})$ and $(\bar{\varphi}^{(0)},\bar{\varphi}^{(1)})$, and using attenuation and (4.27) and (4.28), we find the solvability condition

$$\epsilon^{(1)} = (\epsilon^{(0)})^2\left(\frac{\epsilon^{(0)}-1}{\epsilon^{(0)}}\right)^{3/2}\frac{\oint[\partial\bar{\varphi}^{(0)}/\partial n]^2\,\mathrm{d}A}{\oint\bar{\varphi}^{(0)}(\partial\bar{\varphi}^{(0)}/\partial n)\,\mathrm{d}A}, \tag{4.29}$$

where integrals are taken over the effective metal–vacuum interface. By applying Green's first identity to the denominator it is readily seen that $\epsilon^{(1)} > 0$, i.e. hydrodynamic non-locality results in a surface plasmon blueshift for arbitrary shaped particles.

There are many cases, particularly for highly symmetric configurations, where more than one independent plasmon mode is supported at a single eigenfrequency. The preceding argument is

readily generalized to such cases where $\epsilon^{(0)}$ is N-times degenerate, with distinct eigenpotential pairs $(\varphi_n^{(0)},\bar{\varphi}_n^{(0)})$, where $n=1,2,\ldots,N$. To allow for a general 'local' state, we recast (4.3) as

$$\varphi \sim \sum_{n=1}^{N} \alpha_n \varphi_n^{(0)}(\mathbf{x}) + \delta\varphi^{(1)}(\mathbf{x}) + \cdots \quad \text{and} \quad \bar{\varphi} \sim \sum_{n=1}^{N} \alpha_n \bar{\varphi}_n^{(0)}(\mathbf{x}) + \delta\bar{\varphi}^{(1)}(\mathbf{x}) + \cdots, \tag{4.30}$$

where $\{\alpha_n\}$ is a set of real numbers to be determined together with $\epsilon^{(1)}$. Applying Green's second identity to the $2N$ pairs $(\varphi^{(1)},\varphi_m^{(0)})$ and $(\bar{\varphi}^{(1)},\bar{\varphi}_m^{(0)})$, where $m=1\ldots N$, and using attenuation,

$$[\epsilon^{(0)}]^2 \left(\frac{\epsilon^{(0)}-1}{\epsilon^{(0)}}\right)^{3/2} \sum_{n=1}^{N} \alpha_n \oint \frac{\partial\bar{\varphi}_n^{(0)}}{\partial n}\frac{\partial\bar{\varphi}_m^{(0)}}{\partial n}\,\mathrm{d}A = \epsilon^{(1)} \sum_{n=1}^{N} \alpha_n \oint \bar{\varphi}_m^{(0)}\frac{\partial\bar{\varphi}_n^{(0)}}{\partial n}\,\mathrm{d}A. \tag{4.31}$$

Equation (4.31) is a matrix problem for the eigenvalues $\epsilon^{(1)}$ and the eigenvectors $\{\alpha_n\}$. We shall next apply (4.29) and (4.31) to geometries for which the leading 'local' eigenpotentials and eigenvalues have been obtained in the literature using separation of variables.

(e) The sphere and circular cylinder

Returning to the sphere example of §3, in the local approximation the plasmonic eigenvalues and eigenpotentials of a sphere are particularly simple and are well known to be

$$\epsilon_l^{(0)} = -\frac{l+1}{l}, \quad l=1,2,\ldots \tag{4.32}$$

and

$$\bar{\varphi}_{lm}^{(0)} = r^l Y_{lm}(\theta,\phi), \quad m=-l,\ldots,l, \tag{4.33}$$

where (r,θ,ϕ) are arbitrarily oriented spherical coordinates with origin at the sphere centre and Y_{lm} are spherical harmonics; the external potentials are not required. Since $\epsilon_l^{(0)}$ is $(2l+1)$ degenerate, we must in principal employ (4.31), but the integrals are zero for $n\neq m$ from the orthogonality properties of $\bar{\varphi}_{lm}^{(0)}$. The linear system (4.31), therefore, reduces to (4.29), yielding

$$\epsilon_l^{(1)} = l^{-1}(l+1)^{1/2}(2l+1)^{3/2}, \tag{4.34}$$

with the $(2l+1)$ degeneracy surviving to $O(\delta)$. Note that rewriting (4.32) and (4.34) in terms of frequency using (4.2) yields (3.10).

Consider next the case of a circular cylinder of dimensionless radius 1. Local theory yields just one eigenvalue, $\epsilon^{(0)}=-1$, which is infinitely degenerate with internal eigenpotentials

$$\bar{\varphi}_{m0}^{(0)} = r^m\cos(m\phi) \quad \text{and} \quad \bar{\varphi}_{m1}^{(0)} = r^m\sin(m\phi), \quad m=1,2,\ldots \tag{4.35}$$

Equations (4.31) furnish the system of equations

$$2^{3/2}m\alpha_{mp} = \epsilon^{(1)}\alpha_{mp}, \quad p=0,1, \quad m=1,2,\ldots, \tag{4.36}$$

which has an infinite number of eigenvalue solutions

$$\epsilon_m^{(1)} = 2^{3/2}m, \quad m=1,2,\ldots, \tag{4.37}$$

where for each m the corresponding eigenvector satisfies $\alpha_{np}=0$ for $n\neq m$. Interestingly, at $O(\delta)$ the unique local eigenvalue $\epsilon^{(0)}$ splits into an infinite set of eigenvalues, each remaining only doubly degenerate. The inapplicability of the regular perturbation scheme for large m does not affect the perturbation for small and moderate m owing to the decoupling in (4.31) for different m (but not p) values. Justified suspicion arising from use of (4.31) for infinite degeneracy is mitigated by a comparison with an exact separable solution of the non-local model in polar coordinates.

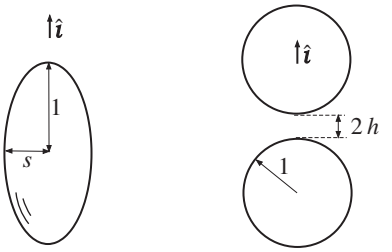

Figure 3. Dimensionless schematics of nanometallic configurations considered in §4 and §5.

(f) Prolate spheroid

As a non-trivial example, consider a prolate spheroid with dimensionless semi-axes 1 and $s<1$ (figure 3). In the local approximation, separation of variables in prolate-spheroidal coordinates [27] provides the eigenvalues as

$$\epsilon_{nm}^{(0)}=\left.\frac{Q_n^{m\prime}(x)P_n^m(x)}{P_n^{m\prime}(x)Q_n^m(x)}\right|_{x=1/\sqrt{1-s^2}},\quad n=1,2,\ldots,\ m=0,1,\ldots,n, \tag{4.38}$$

where P_n^m and Q_n^m are associated Legendre functions of the first and second kind, with a branch cut from $-\infty$ to 1 along the real axis. Eigenvalues with $m=0$ correspond to axisymmetric modes, and are simple; eigenvalues with $m\neq 0$ are non-axisymmetric and are twice degenerate in accordance with the rotational symmetry of the spheroid. In particular, the eigenvalue $\epsilon_{10}^{(0)}$ can be expressed explicitly as[1]

$$\epsilon_{10}^{(0)}=\frac{\ln((1+\sqrt{1-s^2})/(1-\sqrt{1-s^2}))-2s^{-2}\sqrt{1-s^2}}{\ln((1+\sqrt{1-s^2})/(1-\sqrt{1-s^2}))-2\sqrt{1-s^2}}. \tag{4.39}$$

The associated surface plasmon eigenfield is uniform within the metal [27], that is $\bar{\varphi}_{10}^{(0)}=\hat{\boldsymbol{\imath}}\cdot\mathbf{x}$, where $\hat{\boldsymbol{\imath}}$ is a unit vector parallel to the spheroid's major axis. Invoking prolate-spheroidal coordinates to evaluate the integrals in (4.29), the non-local eigenvalue perturbation is found as

$$\epsilon_{10}^{(1)}=\frac{3}{2}[\epsilon_{10}^{(0)}]^2\left(\frac{\epsilon_{10}^{(0)}-1}{\epsilon_{10}^{(0)}}\right)^{3/2}\frac{s}{(1-s^2)^{3/2}}\left[\arctan\frac{\sqrt{1-s^2}}{s}-s\sqrt{1-s^2}\right]. \tag{4.40}$$

Equation (4.40), together with (4.2) and (4.40), provides the blueshift of the fundamental axisymmetric, Fröhlich-type, surface plasmon mode of a prolate spheroid. The latter mode is of special importance in sensing applications [40], as it allows a tuneable plasmon frequency over a broad band and high field enhancements; it is also the only mode which can be effectively excited by light polarized parallel to the axis. The correction (4.40) may be of particular importance for accurately using elongated particles as 'plasmon rulers'. To demonstrate the applicability of (4.40), we have numerically solved, using the commercial finite-element package Comsol Multiphysics®, the problem of a subwavelength (quasi-static) prolate spheroid illuminated by a plane wave polarized parallel to $\hat{\boldsymbol{\imath}}$. In figure 4 we plot, for $s=1, 0.5, 0.25$ and 0.1, the imaginary part of the axial field induced on the symmetry axis at unity distance away from the spheroid tip. The black and blue lines, respectively, depict the local and non-local calculations. The vertical dashed black and blue lines, respectively, mark the eigenfrequency predictions associated with (4.38) and (4.29).

[1]Note that for $x>1$: $P_1^0(x)=x$, $Q_1^0(x)=\frac{1}{2}x\ln((x+1)/(x-1))-1$.

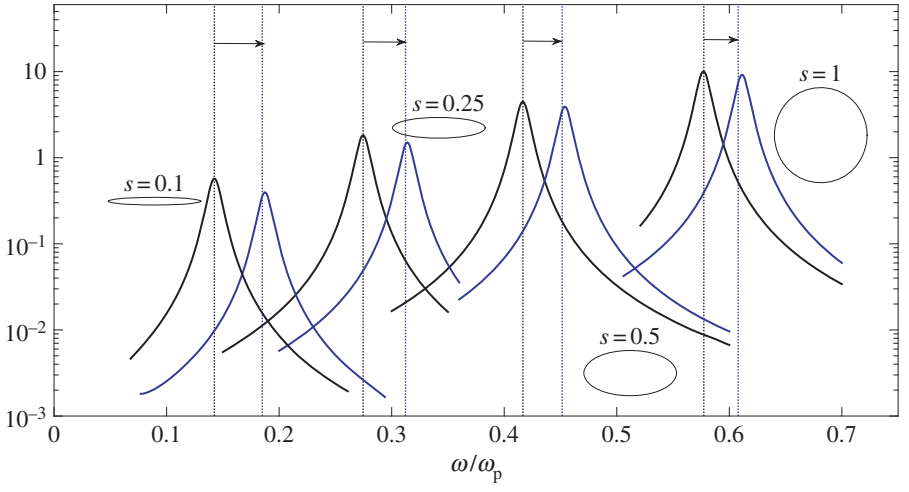

Figure 4. Dimensionless near field $|\mathrm{Im}[\hat{\boldsymbol{\imath}} \cdot \boldsymbol{\nabla}\varphi]|$ external to metallic prolate spheroid ($\gamma/\omega_p = 0.014, \delta = 0.04$) subjected to a plane wave polarized along $\hat{\boldsymbol{\imath}}$, for several values of the slenderness parameter s (the field is probed on the revolution axis at unit distance from the spheroid tip). Black and blue lines are respectively the local and non-local responses from a quasi-static simulation. The vertical dotted black and blue lines, respectively, depict the dipolar resonant frequency predicted from local theory (cf. (4.39)) and our perturbative non-local theory (cf. (4.40)). (Online version in colour.)

Figure 4 demonstrates the familiar geometrical redshift as $s \to 0$ in the local plasmon frequency. Indeed, analysis of the local approximation (4.39) shows that

$$\epsilon^{(0)} \sim -\frac{1}{[\ln(2/s) - 1]s^2} \quad \text{as } s \to 0, \tag{4.41}$$

i.e. in the local approximation the plasmon frequency redshifts rapidly and without bound as $s \to 0$. Adding to (4.41) the small-s asymptotics of the non-local perturbation (4.40), we find, formally,

$$\epsilon \sim \frac{1}{[\ln(2/s) - 1]s^2}\left[-1 + \frac{3\pi}{4}\frac{\delta/s}{\ln(2/s) - 1} + \cdots\right], \quad \delta \ll s \ll 1. \tag{4.42}$$

The asymptotic hierarchy in (4.42) is clearly invalidated when $s = O(\delta)$. Indeed, in this extreme the transverse metal dimension is $O(\lambda_F)$ and we expect non-locality to be appreciable. We next turn to an example where non-locality becomes dominant even though the metal dimensions are strictly $\gg \lambda_F$, owing to a geometric electric-field amplification.

(g) Circular cylindrical dimer

As a final exemplar of the perturbation formula (4.29) consider a pair of identical metallic cylinders of dimensionless radius 1, separated by a gap of dimensionless width $2h$ (figure 3). The 'local' eigenvalues and eigenpotentials are derived in [27] by separation of variables in bipolar coordinates; the eigenpotentials are characterized as being either symmetric or antisymmetric about the plane bisecting the gap. We focus on the antisymmetric modes, known also as the longitudinal or 'bonding' modes, that are particularly important in plasmonic applications owing to their tunability and high field confinement. The relevant eigenvalues are

$$\epsilon_n^{(0)} = -\coth[(n+1)\cosh^{-1}(1+h)], \quad n = 0, 1, 2, \ldots, \tag{4.43}$$

each of which is doubly degenerate with associated bonding modes symmetric and antisymmetric about an axis coinciding with the line of centres. Conveniently, however, the eigenpotentials as given in [27] are orthogonal over the metal–vacuum interface, whereby the system of equations

(4.31) again degenerates to (4.29). Evaluating the integrals in bipolar coordinates, the latter yields

$$\epsilon_n^{(1)} = -(n+1)\epsilon_0^{(0)}[\epsilon_n^{(0)}]^2\left[\frac{\epsilon_n^{(0)}-1}{\epsilon_n^{(0)}}\right]^{3/2}. \tag{4.44}$$

This result is demonstrated in figure 7, which will be discussed in §6.

The bonding modes of a cylindrical dimer redshift as $h \to 0$ analogously to the longitudinal Fröhlich mode of a prolate spheroid as $s \to 0$ (cf. (4.41)). Inspection of (4.43) shows that [41]

$$\epsilon_n^{(0)} \sim -\frac{1}{n+1}\frac{1}{\sqrt{2h}} + O(\sqrt{h}), \quad \text{as } h \to 0. \tag{4.45}$$

Adding to (4.45) the small-h asymptotics of (4.44) we find, formally,

$$\epsilon \sim -\frac{1}{n+1}\frac{1}{\sqrt{2h}} + \frac{\delta}{n+1}\frac{1}{(2h)^{3/2}}, \quad \delta \ll h \ll 1, \tag{4.46}$$

which is no longer asymptotic when $h = O(\delta)$. The breakdown here of the regular eigenvalue expansion (4.1) is, unlike in the spheroid case, linked to a non-metallic rather than a metallic dimension becoming comparable to the screening length.

5. Nearly touching circular cylinders

In this section, we revisit the plasmonic eigenvalue problem for a circular cylindrical dimer (see §4g), this time carrying out an *ab initio* asymptotic analysis in the prevailing case where both h and δ are small. As in §4g, we shall focus on bonding eigenpotentials, which are antisymmetric with respect to the plane bisecting the gap. For $h \gg \delta$, we expect the small-perturbation scheme of §4g to hold; thus, in this case (4.44) is valid to leading order, with non-locality playing only a relatively minor role captured by the second term in (4.46). By contrast, in the strongly non-local case, $h = O(\delta)$, we expect non-locality to affect the plasmon eigenfrequencies at leading order. Before tackling the strongly non-local limit, we shall first in §5a derive the local near-contact asymptotics (4.44), adopting the singular perturbations approach demonstrated in [33] for a sphere dimer (in the local approximation). We shall then find in §5b that this approach extends in a simple way to the strongly non-local case, where an exact analytical approach is intractable.

(a) Weak non-locality: $h \gg \delta$

(i) Local eigenvalue problem

To derive the leading order surface plasmon eigenvalues and eigenpotentials in the near-contact limit $h \ll 1$, with $\delta \ll h$, we disregard non-locality and seek non-trivial eigenpotentials φ and $\bar{\varphi}$ satisfying Laplace equations in the vacuum and metal domains, respectively, along with

$$\varphi = \bar{\varphi}, \quad \frac{\partial\varphi}{\partial n} = \epsilon\frac{\partial\bar{\varphi}}{\partial n} \tag{5.1}$$

as the local interfacial conditions and attenuation of $\varphi \to 0$ at large distances. We introduce cartesian coordinates (x, y), with unit vectors $(\hat{\mathbf{e}}_x, \hat{\mathbf{e}}_y)$, origin at the gap centre, and $\hat{\mathbf{e}}_y$ directed parallel to the line of particle centres (figure 5). Our interest lies in bonding modes satisfying

$$\varphi(x, y) = -\varphi(x, -y) \tag{5.2}$$

and similarly for $\bar{\varphi}$. Note that (5.2) allows us to consider only the half plane $y > 0$, e.g. by prescribing the condition

$$\varphi(x, 0) = 0. \tag{5.3}$$

The scaling of the ϵ eigenvalues as $h \to 0$ follows from arguments similar to those given in [33] and [34]. We define $(x, y) = O(h^{1/2}, h)$ as the gap region, where given the locally parabolic cylinder boundaries the gap separation remains $O(h)$. Assuming $\varphi = O(1)$ there, (5.3) implies an $O(1/h)$

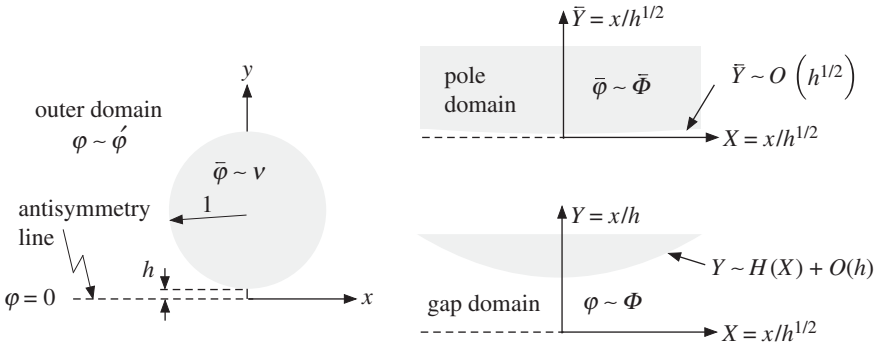

Figure 5. Near-contact asymptotic structure of bonding modes of a circular cylindrical dimer in the local approximation.

transverse gap field. Also, since for $y = O(h)$ and $|x| \gg h^{1/2}$, (5.3) implies $\varphi = O(h)$, and hence for fixed y the gap potential attenuates over $x = O(h^{1/2})$. Considering next the metal side of the gap boundary, continuity of potential implies $\bar{\varphi}$ is $O(1)$ varying rapidly over $O(h^{1/2})$ distances along the boundary. Owing to the apparent unboundedness of the metal domain on such small scales, and the symmetry of Laplace's equation, we expect equally rapid transverse variations in potential, i.e. the transverse pole field is $O(1/h^{1/2})$; we refer to the $O(h^{1/2}) \times O(h^{1/2})$ metal regions as the poles. Substituting the transverse-field scalings in the gap and pole domains into the electric displacement condition at the vacuum–metal interface suggests

$$\epsilon \sim -\zeta\, h^{-1/2}, \tag{5.4}$$

where $\zeta = O(1)$ is a prefactor to be determined. The asymptotic structure of the sought eigenpotentials is closed by noting that, since $|\epsilon| \gg 1$, on $O(1)$ length scales, away from the gap, the metal cylinders must to leading order be at fixed and opposite potentials, say $\pm\mathcal{V}$.

(ii) Asymptotic analysis

More formally, the gap domain is defined to be where the stretched coordinates $X = x/h^{1/2}$ and $Y = y/h$ are $O(1)$ (figure 5), the cylindrical boundaries reading as $Y \sim \pm H(X) + O(h)$, where $H(X) = 1 + \frac{1}{2}X^2$. Expanding the gap potential as $\varphi \sim \Phi(X, Y) + O(h^{1/2})$, Laplace's equation at leading order degenerates to $\partial^2\Phi/\partial Y^2 = 0$, which together with (5.3) shows that

$$\Phi = -E(X)Y. \tag{5.5}$$

The gap field is dominantly transverse with the field distribution $E(X)$ yet to be determined.

Consider next the pole domain within the metal cylinder (e.g. in $y > 0$), where the alternative set of stretched coordinates, X and $\bar{Y} = y/h^{1/2}$, are $O(1)$. With this stretching, the cylinder boundary appears flat, $\bar{Y} \sim O(h^{1/2})$. Expanding the potential there as $\varphi \sim \bar{\Phi}(X, \bar{Y}) + O(h^{1/2})$, Laplace's equations gives

$$\frac{\partial^2\bar{\Phi}}{\partial X^2} + \frac{\partial^2\bar{\Phi}}{\partial \bar{Y}^2} = 0, \tag{5.6}$$

whereas the interfacial conditions (5.1), in conjunction with (5.5), read

$$\bar{\Phi} = -E(X)H(X) \quad \text{and} \quad \zeta\frac{\partial\bar{\Phi}}{\partial\bar{Y}} = E(X), \quad \text{at } \bar{Y} = 0. \tag{5.7}$$

The latter can be combined to form the mixed-type boundary condition

$$\bar{\Phi} + \zeta H(X)\frac{\partial\bar{\Phi}}{\partial\bar{Y}} = 0 \quad \text{at } \bar{Y} = 0. \tag{5.8}$$

Equations (5.6) and (5.8), together with the matching condition $\bar{\Phi} \to \mathcal{V}$ as $X^2 + \bar{Y}^2 \to \infty$, define an effective eigenvalue problem in the half plane $\bar{Y} > 0$, which we shall now solve.

It is convenient to work with the potential deviation $\psi = \bar{\Phi} - \mathcal{V}$, and its Fourier transform,

$$\hat{\psi}(k, \bar{Y}) = \frac{1}{\sqrt{2\pi}} \int_{-\infty}^{\infty} \psi(X, \bar{Y})\, \mathrm{e}^{-\mathrm{i}kX}\, \mathrm{d}X. \tag{5.9}$$

Equations (5.6) and the matching condition at infinity together imply

$$\hat{\psi} = M(k)\, \mathrm{e}^{-|k|\bar{Y}}. \tag{5.10}$$

Fourier transforming the mixed-type boundary condition (5.8), we find that the distribution $M(k)$ is governed by the differential equation

$$(1 - \zeta\,|k|)M(k) + \frac{\zeta}{2}\frac{\mathrm{d}^2}{\mathrm{d}k^2}[|k|M(k)] = -\sqrt{2\pi}\,\mathcal{V}\delta_{\mathrm{D}}(k), \tag{5.11}$$

$\delta_{\mathrm{D}}(k)$ denoting the Dirac-delta function.

It is convenient at this point to consider separately eigenpotentials even and odd in x, for which $M(k)$ is, respectively, even and odd in k. For eigenpotentials even in x we write (5.11) as

$$\frac{\mathrm{d}^2(kM)}{\mathrm{d}k^2} + 2\left(\frac{1}{\zeta} - k\right)M = 0, \quad k > 0, \tag{5.12}$$

together with the condition

$$M(0) = -\frac{\sqrt{2\pi}\,\mathcal{V}}{\zeta}, \tag{5.13}$$

which is obtained by balancing the singularity at $k = 0$. A large-k analysis suggests the substitution $M(k) = \mathrm{e}^{-\sqrt{2}|k|}N(2\sqrt{2}|k|)$, whereby

$$p\frac{\mathrm{d}^2N}{\mathrm{d}p^2} + (2 - p)\frac{\mathrm{d}N}{\mathrm{d}p} - \left(1 - \frac{1}{\sqrt{2}\zeta}\right)N = 0, \quad p = 2\sqrt{2}k > 0. \tag{5.14}$$

Equation (5.14) is identified as the associated Laguerre differential equation. Non-singular solutions consistent with (5.13) and having algebraic growth as $p \to \infty$ exist only when the bracketed term in (5.14) is a non-positive integer, say n, the solution then proportional to $L_n^1(p)$, the nth associated Laguerre polynomial of order one [42]. Thence the leading-order eigenvalues are

$$\zeta_n = \frac{1}{\sqrt{2}(1 + n)}, \quad n = 0, 1, 2, \ldots. \tag{5.15}$$

Noting that $L_n^1(0) = n + 1$, the corresponding eigenfunctions $M = M_n^e(k)$ satisfying (5.13) are

$$M_n^e(k) = -2\sqrt{\pi}\,\mathcal{V}\, \mathrm{e}^{-\sqrt{2}|k|}L_n^1(2\sqrt{2}|k|); \tag{5.16}$$

the outer voltage $\mathcal{V}$ is an arbitrary multiplicative factor determining the magnitude of the mode.

As prompted, there are also eigensolutions of (5.11) that are odd in k, with $\mathcal{V} = 0$. If M is to remain finite as $|k| \to 0$ (this is justified in the discussion below (5.21)), then again solutions with appropriate behaviour as $|k| \to \infty$ are only possible for ζ eigenvalues given by (5.15), which are accordingly degenerate as already mentioned in §4g. The odd transformed solutions are readily seen to be the discontinuous variants of (5.16),

$$M_n^o(k) = -2\sqrt{\pi}\,\mathcal{D}\mathrm{sg}(k)\, \mathrm{e}^{-\sqrt{2}|k|}L_n^1(2\sqrt{2}|k|), \tag{5.17}$$

where, with $\mathcal{V} = 0$, we take $\mathcal{D}$ as an arbitrary multiplicative factor.

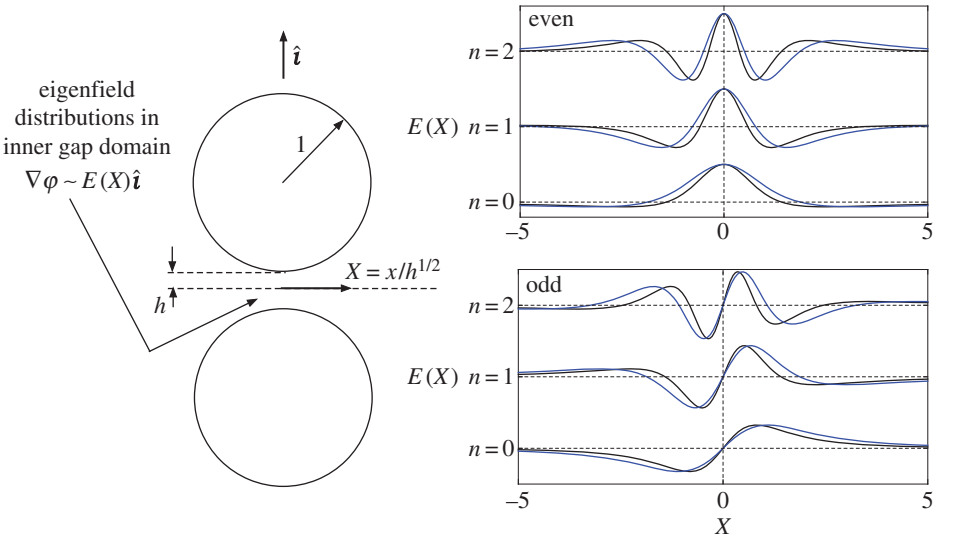

Figure 6. Gap-field distributions $E(X)$ (cf. (5.5)) corresponding to the first three resonance frequencies. Each eigenfrequency is doubly degenerate with eigenfields even and odd in X. The black lines are the 'local' distributions (5.19) and (5.20). The blue lines depict the 'non-local' renormalized distributions (cf. (5.34)) at the blueshifted frequencies (5.35), for $\tau = \delta/h = 0.75$. (Online version in colour.)

The eigenpotentials may be readily calculated by explicit Fourier inversion. Of most interest perhaps is the x-distribution of the gap field (cf. (5.5)),

$$E_n^{e/o}(X) = -\frac{\zeta_n}{\sqrt{2\pi}} \int_{-\infty}^{\infty} |k| M_n^{e/o}(k)\, \mathrm{e}^{\mathrm{i}kX}\, \mathrm{d}k. \tag{5.18}$$

Noting that $L_0^1(p) = 1, L_1^1(p) = 2 - p$ and $L_2^1(p) = 3 - 3p + p^2/2$, the first three even gap-field distributions are

$$\frac{E_0^e(X)}{\mathcal{V}} = \frac{2(2 - X^2)}{(2 + X^2)^2}, \quad \frac{E_1^e(X)}{\mathcal{V}} = -\frac{2(4 - 12X^2 + X^4)}{(2 + X^2)^3},$$
$$\frac{E_2^e(X)}{\mathcal{V}} = -\frac{2(-8 + 60X^2 - 30X^4 + X^6)}{(2 + X^2)^4}, \ldots, \tag{5.19}$$

while the first three odd ones are

$$\frac{E_0^o(X)}{(i\mathcal{D})} = \frac{4\sqrt{2}X}{(2 + X^2)^2}, \quad \frac{E_1^o(X)}{(i\mathcal{D})} = \frac{8\sqrt{2}X(X^2 - 2)}{(2 + X^2)^3},$$
$$\frac{E_2^o(X)}{(i\mathcal{D})} = \frac{4\sqrt{2}X(12 - 20X^2 + 3X^4)}{(2 + X^2)^4}, \ldots. \tag{5.20}$$

The above distributions are depicted by the black lines in figure 6. We note that the even modes are somewhat less strongly confined in the gap than the odd ones. In fact, in the three-dimensional case of a sphere dimer, the attenuation of the axisymmetric modes (analogous to the even modes here) is so slow that the eigenfrequencies cannot be determined by analysing the gap and pole domains separately from the particle-scale field distribution [33].

To complete the description of the eigenpotentials, we consider the 'outer' vacuum domain, at $O(1)$ distances away from the gap where to leading order the cylinders appear to be touching. For eigenpotentials even in x, alluding to the analysis of nearly touching perfectly conducting cylinders (see appendix in [43]), it is readily verified that the outer vacuum potential is

$$\varphi \sim \acute{\varphi} + \cdots, \quad \acute{\varphi} = 2\mathcal{V}\frac{y}{x^2 + y^2}. \tag{5.21}$$

Indeed, this distribution satisfies Laplace's equation, is even in x and odd in y, attenuates at large distances and takes the value $\mathcal{V}$ at the approximate boundary of the upper cylinder. Importantly, (5.21) asymptotically matches with the gap region. Thus, writing $\acute{\phi}$ in terms of the inner gap coordinates and expanding for small h gives $\sim 2\mathcal{V}Y/X^2$, which in turn implies $E(X) \sim -2\mathcal{V}/X^2$; it is easily seen that the latter is the large $|X|$ behaviour of the gap distributions (5.19) for all n. Consider next the eigenpotentials odd in x, for which $\mathcal{V} = 0$. Equations (5.20) imply that as $X \to \infty$, $E(X) \sim O(1/X^3)$ and hence from (5.5) the potential is $O(Y/X^3)$. Matching in turn suggests the outer potential is $O(h^{1/2})$ small. The seemingly trivial $O(1)$ outer problem involving Laplace's equation, a homogeneous Dirichlet condition on the cylinder boundaries, and attenuation at large distances, actually possesses solutions which are singular at the origin [43]; these, however, are too singular to match any allowable inner solution; this in turn justifies *a posteriori* our assumption that $M(k)$ is finite at the origin.

(b) Strong non-locality: $h = O(\delta)$

With the near-contact asymptotics in the local approximation determined, we proceed to consider the strongly non-local limit, where the gap width is small compared with the cylinder radius and comparable to the non-local screening length, i.e. $1 \gg h = O(\delta)$. From the coarse-graining procedure of §4b, we expect that away from the gap, where the potential is $O(1)$, say, and varies over $O(1)$ length scales, there will be an electron-charge boundary layer of thickness $O(\delta) = O(h)$ wherein $q = O(1)$. Hence, away from the gap we have to leading order the standard local conditions connecting the bulk vacuum potential and bulk metal potential. Moreover, assuming, subject to *a posteriori* confirmation, that ϵ retains the scaling (5.4), the outer metal-bulk potential is, as in §5a, uniform to leading order. In the vicinity of the gap, however, the situation is quite different. We still expect an electron-charge boundary layer of thickness $O(\delta)$, narrow relative to the pole domain studied in §5a; however, the comparably strong $O(1/h)$ transverse field in the gap implies through the no-flux boundary condition (third of (2.14)) that $q = O(1/h)$ in the boundary-layer segment interacting with the gap; this increase in charge density results in a reshuffle of the asymptotics and consequently in the promotion of non-locality to leading order.

We begin as in §5a by postulating a gap potential in the form $\varphi \sim \Phi + O(h^{-1/2})$, where $\Phi = -E(X)Y$. In describing the electron-charge layer adjacent to the gap region, we continue to employ the gap coordinates X, Y, with now $Y > H(X) + O(h)$. The scaling arguments given above suggest the boundary-layer expansions

$$q \sim h^{-1}Q_{-1} + h^{-1/2}Q_{-1/2} + \cdots, \quad \chi \sim T_0 + h^{1/2}T_{1/2} + \cdots, \tag{5.22}$$

where, as in §4b, it is convenient to consider χ instead of the potential $\bar{\varphi}$. According to (5.4),

$$\frac{\epsilon}{\epsilon - 1} \sim 1 + O(h^{1/2}) \quad \text{and} \quad \frac{1}{\epsilon - 1} \sim -\frac{1}{\zeta}h^{1/2} + O(h). \tag{5.23}$$

Taking $\tau = \delta/h$ as an $O(1)$ parameter, we require the leading-order governing equations that follow from (2.15), together with that governing $T_{1/2}$,

$$\tau^2 \frac{\partial^2 Q_{-1}}{\partial Y^2} = Q_{-1}, \quad \frac{\partial^2 T_0}{\partial Y^2} = 0 \quad \text{and} \quad \tau \frac{\partial^2 T_{1/2}}{\partial Y^2} = -\frac{Q_{-1}}{\zeta}. \tag{5.24}$$

Similarly, the leading-order interfacial conditions follow from (2.16) as

$$\frac{\partial Q_{-1}}{\partial Y} = \frac{1}{\tau}E(X), \quad \frac{\partial T_0}{\partial Y} = 0, \quad E(X)H(X) = \tau Q_{-1} - T_0 \quad \text{at } Y = H(X), \tag{5.25}$$

and we will also need the next-order condition

$$\frac{\partial T_{1/2}}{\partial Y} = 0 \quad \text{at } Y = H(X). \tag{5.26}$$

Note that curvature is absent in (5.26) as the relative errors in approximating the boundary as $Y \sim H(X)$ and the normal derivative as $\partial/\partial n \sim (1/h)\partial/\partial Y$ are both $O(h)$. Additional conditions

arise from matching with the transversally wider pole region, where q is exponentially small and the potential is expanded as $\bar{\varphi} \sim \bar{\Phi}(X, \bar{Y}) + O(h^{1/2})$, $\bar{\Phi}(X, \bar{Y})$ satisfying Laplace's (5.6) and the matching condition at infinity. First, the exponential order of q implies that

$$Q_{-1}, Q_{-1/2}, \ldots \quad \text{as } Y \to \infty. \tag{5.27}$$

Second, assuming the pole potential is regular as $\bar{Y} \to 0$, expanding the leading term $\bar{\Phi}$ and rewriting in boundary-layer coordinates (X, Y) gives

$$\Phi(X, \bar{Y} = 0) + h^{1/2} Y \frac{\partial \bar{\Phi}}{\partial \bar{Y}}(X, \bar{Y} = 0) + \cdots, \tag{5.28}$$

whereby matching rules imply the conditions

$$T_0 \sim \Phi(X, \bar{Y} = 0) + o(1) \quad \text{and} \quad T_{1/2} \sim Y \frac{\partial \bar{\Phi}}{\partial \bar{Y}}(X, \bar{Y} = 0) + o(Y), \quad \text{as } Y \to \infty. \tag{5.29}$$

Integrating (5.24) in conjunction with (5.25) and (5.27), we find

$$Q_{-1} = -E(X) \mathrm{e}^{-[Y - H(X)]/\tau} \quad \text{and} \quad T_0 = -E(X)[H(X) + \tau]. \tag{5.30}$$

Next, integrating the third equation of (5.24) using (5.30) and (5.26) gives the asymptotic behaviour

$$\frac{\partial T_{1/2}}{\partial Y} \sim \frac{1}{\zeta} E(X) \quad \text{as } Y \to \infty. \tag{5.31}$$

This, together with (5.29), (5.30) and (5.31), yields the effective conditions connecting the pole and gap regions,

$$\bar{\Phi} = -[H(X) + \tau] E(X), \quad \frac{\partial \bar{\Phi}}{\partial \bar{Y}} = \frac{1}{\zeta} E(X), \quad \text{at } \bar{Y} = 0, \tag{5.32}$$

that combine giving a modified mixed boundary condition governing the pole region [cf. (5.8)],

$$\zeta [H(X) + \tau] \frac{\partial \bar{\Phi}}{\partial \bar{Y}} + \bar{\Phi} = 0 \quad \text{at } \bar{Y} = 0. \tag{5.33}$$

Together with (5.6) and the matching at infinity, the effective condition (5.33) defines a new problem governing the metal-pole potential $\bar{\Phi}$. Remarkably, this problem is identical to that which we had found in the local case, other than the addition of τ to $H(X)$ in (5.33). In dimensional terms, this corresponds to an effective widening of the gap by $2\lambda_{\mathrm{F}}$, as intuitively argued in [34]; the 'local' pole problem of §5a is recovered by making the transformations

$$X \to \sqrt{1 + \tau} X, \quad \bar{Y} \to \sqrt{1 + \tau} \bar{Y} \quad \text{and} \quad \zeta \to \frac{\zeta}{\sqrt{1 + \tau}}. \tag{5.34}$$

As a consequence, and using (5.15) and (5.4), we find the non-local eigenvalues as

$$\epsilon_n \sim -\frac{1}{\sqrt{2(h + \delta)}} \frac{1}{1 + n}, \quad n = 0, 1, 2, \ldots, \tag{5.35}$$

which is a renormalization of the singular local-theory eigenfrequencies [34]. From (5.34), the eigenmodes in the non-local case too are renormalized variants of the local ones, see the gap-field distributions in figure 6.

In figure 7, the blue dashed-dotted line depicts the fundamental ($n = 0$) surface plasmon frequency predicted by (5.35), together with (2.8) and (5.4), in the case of a gold dimer. The parameter set ($a = 10\,\mathrm{nm}$, $\hbar\omega_{\mathrm{p}} = 3.3\,\mathrm{eV}$, $\beta = 0.0036c$, hence $\delta = 0.0215$) is chosen in order to compare with the numerical data of Luo *et al.* [25], extracted here using a plot digitizer and added as symbols in figure 7. Also shown is the exact local result (4.43), black line, the local near-contact asymptotics (5.15), black dashed-dotted, the perturbation result (4.44) derived in §4 for $h = O(1)$, blue dashed, and a uniformly valid approximation to be discussed in the next section, blue line. It should be noted that the error in (5.35) is expected to asymptotically vanish as h and δ become small; since δ is held constant in figure 7, the small error persisting as $h \to 0$ is not surprising.

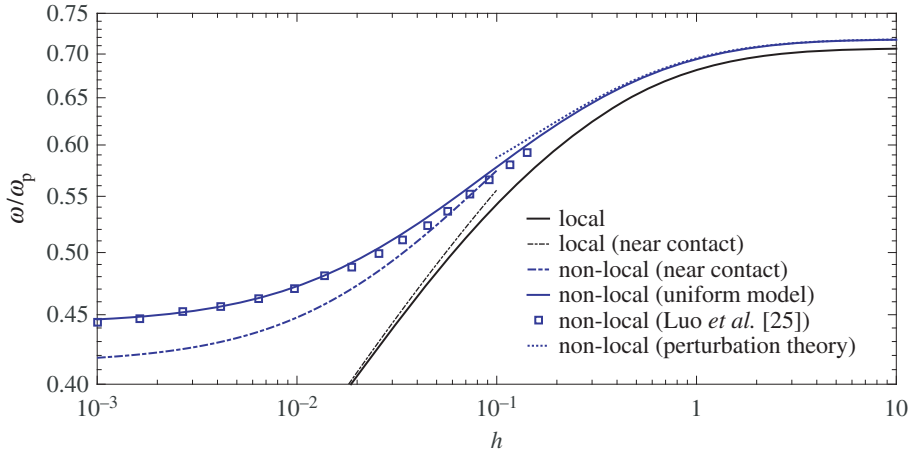

Figure 7. Fundamental surface plasmon bonding-mode of a gold circular cylindrical dimer ($a = 10$ nm, $\hbar\omega_p = 3.3$ eV, $\beta = 0.0036c$, giving $\lambda = 0.215$ nm and $\delta = 0.0215$). See text for details on the various data and approximations shown. (Online version in colour.)

6. A 'uniform' coarse-grained model

Our analysis has proceeded in two complementary routes: in §4, we carried out an asymptotic coarse graining procedure valid for smooth single-scale metallic particles of otherwise arbitrary shape, while in §5, we performed an *ab initio* asymptotic analysis of the near-contact limit of the cylindrical-dimer configuration (in which limit the former approach fails). A 'uniform' macroscale model, from which both approaches follow as special cases, can be obtained by solving Laplace's equation for the vacuum potential φ and the metal-bulk potential $\bar{\varphi}$, in conjunction with the leading- and first-order effective interfacial conditions (4.27) and (4.28) derived in §4 fused together, i.e.

$$\varphi - \bar{\varphi} \sim \delta \left(\frac{\epsilon - 1}{\epsilon} \right)^{3/2} \frac{\partial \varphi}{\partial n}, \quad \frac{\partial \varphi}{\partial n} \sim \epsilon \frac{\partial \bar{\varphi}}{\partial n}. \tag{6.1}$$

Evidently, for single-scale particles (6.1) yield blueshifted eigenfrequencies that are asymptotically identical to those predicted by the perturbation scheme of §4. Less obviously, for multiple-scale configurations having narrow gaps, (6.1) again leads to the correct leading-order asymptotics as found in §5. In the latter scenario, non-locality is most appreciable in the gap region, where owing to the geometrically enhanced gap field the seemingly small potential discontinuity in (6.1) is promoted to leading order. Explicitly, as $h \to 0$, we know that for bonding modes $|\epsilon| \gg 1$ and hence $(\epsilon - 1)/\epsilon \sim 1$; thus the second of (6.1) becomes $\varphi - \bar{\varphi} \sim \delta \partial\varphi/\partial n$. On the other hand, from the gap-scale analysis in §5 at the vacuum–metal interface $\varphi \sim -E(X)H(X)$ and $\partial\varphi/\partial n \sim h^{-1}E(X)$. We therefore see that (6.1) are to leading order asymptotically identical with the effective conditions (5.32). In figure 7, showing the fundamental bonding-mode eigenfrequency of a cylindrical dimer, the solid blue line depicts the prediction obtained using (6.1). At moderate h, the latter agrees with the perturbative result (4.44). At small h, the new prediction agrees very well with the data of Luo *et al.* [25] and reasonably well with the renormalized near-contact asymptotics (5.35); as already explained in §5, the finiteness of δ prevents the error in (5.35) from vanishing as $h \to 0$.

Importantly, the effective interfacial conditions (6.1) apply also to excitation problems. The coarse-graining perturbation scheme of §4, in its original form, breaks down at frequencies close to resonant values as, under resonance conditions, there are two small parameters: δ, which together with geometry determines the resonance frequency in the absence of losses, and

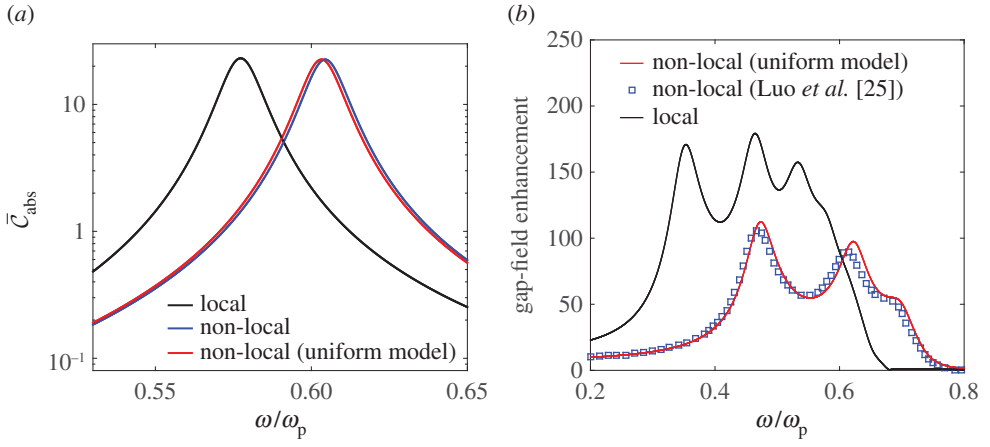

Figure 8. (*a*) Normalized absorption cross section (3.4) of a nanometallic sphere under plane-wave illumination in the quasi-static limit—same parameters as in figure 1. Black and blue lines, respectively, depict the local-theory prediction (3.2) and the non-local-theory prediction (3.5). Red line depicts the prediction (6.2) of the uniform local-analogue model (6.1). (*b*) Field enhancement at the centre of a 0.2 nm wide gap between a pair of gold cylinders of radius $a = 10$ nm ($h = 0.01$), under plane-wave illumination with incident field polarized along the line of centres; same material parameters as in figure 7. Black line, solution of local model; red line, solution of the uniform local-analogue model (6.1); symbols, numerical data extracted from Luo *et al.* [25] with a plot digitizer. (Online version in colour.)

$\mathrm{Im}[\epsilon]/\mathrm{Re}[\epsilon]$, which governs the level of plasmonic enhancement at resonance. In the perturbation scheme of §4, the leading-order description would resonate at the 'local' eigenfrequencies rather than the blueshifted ones, thereby overpowering the $O(\delta)$ correction. A rigorous asymptotic procedure addressing the smallness of both parameters could be carried out be separately considering resonant and non-resonant frequency regimes, or using the method of strained coordinates [35]. The fused conditions (6.1), which uniformly capture the leading non-local effect at resonance, provide a simpler path—asymptotically sound, but admittedly not exploiting at all the smallness of $\mathrm{Im}[\epsilon]/\mathrm{Re}[\epsilon]$ towards simplification, as e.g. in the local analysis of Schnitzer *et al.* [34].

As an example, consider the problem of plane-wave excitation of a metallic nanosphere, already solved in §3 by exact separation of variables of the hydrodynamic Drude model. Employing the simpler local-analogue model with interfacial conditions (6.1), we readily find the dimensionless induced-dipole moment as (cf. (3.2))

$$\mu \approx \frac{\epsilon - 1 - \epsilon\delta[(\epsilon-1)/\epsilon]^{3/2}}{\epsilon + 2 + 2\epsilon\delta[(\epsilon-1)/\epsilon]^{3/2}}. \tag{6.2}$$

The excellent agreement of (6.2) with (3.2) for small δ values is demonstrated in figure 8*a*, where the normalized absorption cross section (3.4) of a metallic nanosphere under plane-wave illumination is plotted as a function of frequency. For a less trivial application of the uniform model, consider the scenario of plane-wave illumination of a metallic circular cylindrical dimer, with the incident electric field polarized along the line of centres. Figure 8*b* compares as a function of frequency the field enhancement in the gap as predicted by the local model (black line), the uniform model (red line) and numerical data of Luo *et al.* [25]; material parameters and the gap-width parameter $h = 0.01$ were chosen to match the latter simulation. The local solution was obtained in [27] by separation of variables in bipolar coordinates. For the uniform model, owing to the form of (6.1) separation of variables yields a system of algebraic equations which needs to be solved numerically (we omit the details). It should also be noted that the simulations in [25] are retarded, whereas the former two approaches are quasi-static.

7. Recapitulation and concluding remarks

The smallness of the non-local screening length λ_F relative to characteristic nanometer scales of plasmonic structures allows, through asymptotic analysis of the hydrodynamic Drude model, to extract in simple form the essential effects of non-locality on Surface plasmon resonance. Thus, together with our previous study [34], the present paper provides a general theory relating blueshifted surface plasmon eigenfrequencies in the non-local case with eigenfrequencies and eigenmodes in the local approximation.

In applying the theory, it is important to distinguish between two cases. For nanometric structures characterized by a single length scale a (or multiple length scales all $\gg \lambda_F$), the blueshifts are asymptotically small, $\Delta\omega/\omega_p = O(\lambda_F/a)$, and the perturbation $\Delta\omega = \omega_{nonloc} - \omega_{loc}$ is given by a quadrature over the corresponding unperturbed local eigenmode (4.29). In dimensional form, and using (4.2), the perturbation formula reads

$$\frac{\Delta\omega}{\omega_p} \sim \frac{\lambda_F}{2} \frac{\oint |\bar{\mathbf{E}} \cdot \hat{\mathbf{n}}|^2 \, dA}{\int |\bar{\mathbf{E}}|^2 \, dV} \sqrt{\frac{\omega_p^2}{\omega_{loc}^2} - 1}, \tag{7.1}$$

where $\bar{\mathbf{E}}$ denotes the local eigenmode field distribution within the metal domain, and the integrals in the numerator and denominator are, respectively, over the surface and volume of the metal domains. For a degenerate unperturbed eigenfrequency the perturbation consists of a set of equations (4.31), which, however, in most cases reduces to (7.1). We have successfully demonstrated the efficacy of this perturbation theory by deriving closed-form blueshift formulae for spheres (4.34), cylinders (4.37), prolate spheroids (4.40) and circular cylindrical dimers (4.44). Whereas in these cases the local eigenmodes are known analytically, it is clear that many more configurations can be studied via (7.1) by harnessing standard numerical schemes and packages for calculating eigenmodes in the local approximation [31,44,45].

The second case entails plasmonic structures characterized by multiple length scales, one of these being $O(\lambda_F)$. In such cases, the perturbation formula (7.1) may fail, as (4.42) and (4.46) show explicitly in the respective extreme cases of a slender elongated body of thickness $O(\lambda_F)$ and a nanowire dimer with an $O(\lambda_F)$ gap width. The latter case falls under the general framework of Schnitzer *et al.* [34], where the eigenfrequencies of gap bonding modes in the near-contact limit are captured by a renormalization of the singular redshift predicted by local theory. In this paper we corroborated this result by carrying out a detailed asymptotic analysis of the near-contact limit of a circular cylindrical dimer (radius a, gap width d). In agreement with Schnitzer *et al.* [34], the analysis showed the eigenfrequencies of the bonding modes to be

$$\frac{\omega_{loc}}{\omega_p} \sim (1+n)^{1/2} \left(\frac{d}{a}\right)^{1/4} \quad \text{and} \quad \frac{\omega_{nonloc}}{\omega_p} \sim (1+n)^{1/2} \left(\frac{d+2\lambda_F}{a}\right)^{1/4}, \quad n = 0, 1, 2, \ldots, \tag{7.2}$$

in the local and non-local levels of description, respectively.

Both the perturbation formula for single-scale geometries (7.1) and the near-contact renormalization (7.2) hinge upon the narrowness of the electron-charge boundary layers forming at metal–vacuum interfaces relative to field and charge variations along those interfaces. This separation of scales is evident for surface plasmons of single scale particles (excluding high-order modes). For bonding gap modes in the near-contact limit, however, this is less clear, since the near-field is highly confined to the vicinity of the gap. Nevertheless, as argued via scaling arguments in [34], and demonstrated herein by the detailed analysis of §5, the $O(\lambda_F)$-thick boundary layer remains thin relative to the transversal extent of the 'pole' metal region wherein the field is confined. Indeed, the latter is $O[(da)^{1/2}]$ in the absence of non-locality, and $O[(d+2\lambda_F)^{1/2}a^{1/2}]$ in the strongly non-local limit $d = O(\lambda_F)$; hence, the separation of scales prevails all the way up to the theoretical redshift saturation.

The above scale separation enables an asymptotic coarse graining procedure, where the physics of the narrow electron-charge layer are replaced by a set of effective 'local-analogue' interfacial conditions. In [34], we put forward such an effective coarse-grained 'local-analogue'

eigenvalue problem based on scaling arguments and an intuitive one-dimensional analysis. That effective problem consists of finding quasi-static fields $\bar{\mathbf{E}}$ and $\mathbf{E}$ that are solenoidal in the metal and vacuum domains, respectively, with $\mathbf{E}$ attenuating at large distances, and the fields satisfying the effective interfacial conditions

$$\varphi' - \bar{\varphi}' \sim \lambda_{\mathrm{F}} \left(\frac{\epsilon - 1}{\epsilon} \right)^{3/2} \frac{\partial \varphi}{\partial n} \quad \text{and} \quad \frac{\partial \varphi'}{\partial n} \sim \epsilon \frac{\partial \bar{\varphi}'}{\partial n}, \tag{7.3}$$

where ϵ is the relative Drude permittivity (2.8), and φ' and $\bar{\varphi}'$ are electric potentials such that $\mathbf{E} = \mathrm{Re}[-\boldsymbol{\nabla}\varphi' \exp(-\mathrm{i}\omega t)]$ and $\bar{\mathbf{E}} = \mathrm{Re}[-\boldsymbol{\nabla}\bar{\varphi}' \exp(-\mathrm{i}\omega t)]$. Here we have substantiated this model, clarifying its validity and asymptotic accuracy under various circumstances, including plasmonic excitation problems. In particular, using the method of matched asymptotic expansions, we systematically derived the above model for the surface plasmon modes of single-scale particles. In that case, the relative effect of non-locality is $O(\lambda_{\mathrm{F}}/a)$ while the relative error of the model is $O(\lambda_{\mathrm{F}}^2/a^2)$. We further showed that the above model correctly furnishes the leading-order description of gap bonding modes in the near-contact limit, where non-locality is no longer a small perturbation. Thus, for a dimer configuration the effective conditions (7.3) encapsulate the leading-order effect of non-locality across all gap widths.

Data accessibility. All data accompanying this publication are available within the publication and are generated using standard routines in Matlab® and Comsol Multiphysics®.

Authors' contributions. All authors contributed to the conception and design of the model, interpretation of the results and writing the article. The majority of the analysis was done by O.S. All authors have given their final approval of the version to be published.

Competing interests. We have no competing interests.

Funding. R.V.C. and S.A.M. acknowledge funding from the Engineering and Physical Sciences Research Council via Programme grant EP/L024926/1. S.A.M. acknowledges further support from the Royal Society and from the Lee-Lucas Chair that he holds. One author holds an 'International Exchanges Scheme grant'.

References

1. Maier SA. 2007 *Plasmonics: fundamentals and applications*. Berlin, Germany: Springer Science & Business Media.
2. Schuller JA, Barnard ES, Cai W, Jun YC, White JS, Brongersma ML. 2010 Plasmonics for extreme light concentration and manipulation. *Nat. Mater.* **9**, 193–204. (doi:10.1038/nmat2630)
3. Ciracì C, Hill RT, Mock JJ, Urzhumov Y, Fernández-Domínguez AI, Maier SA, Pendry JB, Chilkoti A, Smith DR. 2012 Probing the ultimate limits of plasmonic enhancement. *Science* **337**, 1072–1074. (doi:10.1126/science.1224823)
4. Raza S, Wubs M, Bozhevolnyi SI, Mortensen NA. 2015 Nonlocal study of ultimate plasmon hybridization. *Opt. Lett.* **40**, 839–842. (doi:10.1364/OL.40.000839)
5. David C, García de Abajo FJ. 2011 Spatial nonlocality in the optical response of metal nanoparticles. *J. Phys. Chem. C* **115**, 19 470–19 475. (doi:10.1021/jp204261u)
6. Ciracì C, Pendry JB, Smith DR. 2013 Hydrodynamic model for plasmonics: a macroscopic approach to a microscopic problem. *Chem. Phys. Chem.* **14**, 1109–1116. (doi:10.1002/cphc.201200992)
7. Raza S, Stenger N, Kadkhodazadeh S, Fischer SV, Kostesha N, Jauho AP, Burrows A, Wubs M, Mortensen NA. 2013 Blueshift of the surface plasmon resonance in silver nanoparticles studied with eels. *Nanophotonics* **2**, 131–138. (doi:10.1515/nanoph-2012-0032)
8. Christensen T, Yan W, Raza S, Jauho AP, Mortensen NA, Wubs M. 2014 Nonlocal response of metallic nanospheres probed by light, electrons, and atoms. *ACS Nano* **8**, 1745–1758. (doi:10.1021/nn406153k)
9. Mortensen NA, Raza S, Wubs M, Søndergaard T, Bozhevolnyi SI. 2014 A generalized non-local optical response theory for plasmonic nanostructures. *Nat. Commun.* **5**, 3809. (doi:10.1038/ncomms4809)
10. Raza S, Bozhevolnyi SI, Wubs M, Mortensen NA. 2015 Nonlocal optical response in metallic nanostructures. *J. Phys. Condens. Matter* **27**, 183204. (doi:10.1088/0953-8984/27/18/183204)
11. Zuloaga J, Prodan E, Nordlander P. 2009 Quantum description of the plasmon resonances of a nanoparticle dimer. *Nano Lett.* **9**, 887–891. (doi:10.1021/nl803811g)

12. Esteban R, Borisov AG, Nordlander P, Aizpurua J. 2012 Bridging quantum and classical plasmonics with a quantum-corrected model. *Nat. Commun.* **3**, 825. (doi:10.1038/ncomms1806)
13. Scholl JA, Koh AL, Dionne JA. 2012 Quantum plasmon resonances of individual metallic nanoparticles. *Nature* **483**, 421–427. (doi:10.1038/nature10904)
14. Marinica DC, Kazansky AK, Nordlander P, Aizpurua J, Borisov AG. 2012 Quantum plasmonics: nonlinear effects in the field enhancement of a plasmonic nanoparticle dimer. *Nano Lett.* **12**, 1333–1339. (doi:10.1021/nl300269c)
15. Savage KJ, Hawkeye MM, Esteban R, Borisov AG, Aizpurua J, Baumberg JJ. 2012 Revealing the quantum regime in tunnelling plasmonics. *Nature* **491**, 574–577. (doi:10.1038/nature11653)
16. Scholl JA, García-Etxarri A, Koh AL, Dionne JA. 2013 Observation of quantum tunneling between two plasmonic nanoparticles. *Nano Lett.* **13**, 564–569. (doi:10.1021/nl304078v)
17. Haus JW, de Ceglia D, Vincenti MA, Scalora M. 2014 Quantum conductivity for metal–insulator–metal nanostructures. *J. Opt. Soc. Am. B* **31**, 259–269. (doi:10.1364/JOSAB.31.000259)
18. Toscano G, Straubel J, Kwiatkowski A, Rockstuhl C, Evers F, Xu H, Mortensen NA, Wubs M. 2015 Resonance shifts and spill-out effects in self-consistent hydrodynamic nanoplasmonics. *Nat. Commun.* **6**, 7132. (doi:10.1038/ncomms8132)
19. Zapata Herrera M, Aizpurua J, Kazansky AK, Borisov AG. 2016 Plasmon response and electron dynamics in charged metallic nanoparticles. *Langmuir* **32**, 2829–2840. (doi:10.1021/acs.langmuir.6b00112)
20. Ciracì C, Urzhumov Y, Smith DR. 2013 Effects of classical nonlocality on the optical response of three-dimensional plasmonic nanodimers. *J. Opt. Soc. Am. B* **30**, 2731–2736. (doi:10.1364/JOSAB.30.002731)
21. Luo Y, Zhao R, Pendry JB. 2014 Van der Waals interactions at the nanoscale: the effects of nonlocality. *Proc. Natl Acad. Sci. USA* **111**, 18 422–18 427. (doi:10.1073/pnas.1420551111)
22. García de Abajo FJ. 2008 Nonlocal effects in the plasmons of strongly interacting nanoparticles, dimers, and waveguides. *J. Phys. Chem. C* **112**, 17 983–17 987. (doi:10.1021/jp807345h)
23. Fernández-Domínguez AI, Zhang P, Luo Y, Maier SA, García-Vidal FJ, Pendry JB. 2012 Transformation-optics insight into nonlocal effects in separated nanowires. *Phys. Rev. B* **86**, 241110. (doi:10.1103/PhysRevB.86.241110)
24. Fernández-Domínguez AI, Wiener A, García-Vidal FJ, Maier SA, Pendry JB. 2012 Transformation-optics description of nonlocal effects in plasmonic nanostructures. *Phys. Rev. Lett.* **108**, 106802. (doi:10.1103/PhysRevLett.108.106802)
25. Luo Y, Fernández-Domínguez A, Wiener A, Maier SA, Pendry JB. 2013 Surface plasmons and nonlocality: a simple model. *Phys. Rev. Lett.* **111**, 093901. (doi:10.1103/PhysRevLett.111.093901)
26. Stella L, Zhang P, García-Vidal FJ, Rubio A, García-González P. 2013 Performance of nonlocal optics when applied to plasmonic nanostructures. *J. Phys. Chem. C* **117**, 8941–8949. (doi:10.1021/jp401887y)
27. Klimov V. 2014 *Nanoplasmonics*. Boca Raton, FL: CRC Press.
28. McMahon JM, Gray SK, Schatz GC. 2009 Nonlocal optical response of metal nanostructures with arbitrary shape. *Phys. Rev. Lett.* **103**, 097403. (doi:10.1103/PhysRevLett.103.097403)
29. McMahon JM, Gray SK, Schatz GC. 2010 Calculating nonlocal optical properties of structures with arbitrary shape. *Phys. Rev. B* **82**, 035423. (doi:10.1103/PhysRevB.82.035423)
30. Yan W, Mortensen NA, Wubs M. 2013 Green's function surface-integral method for nonlocal response of plasmonic nanowires in arbitrary dielectric environments. *Phys. Rev. B* **88**, 155414. (doi:10.1103/PhysRevB.88.155414)
31. Mayergoyz ID, Fredkin DR, Zhang Z. 2005 Electrostatic (plasmon) resonances in nanoparticles. *Phys. Rev. B* **72**, 155412. (doi:10.1103/PhysRevB.72.155412)
32. Tserkezis C, Maack JR, Liu Z, Wubs M, Mortensen NA. 2016 Robustness of the far-field response of nonlocal plasmonic ensembles. *Sci. Rep.* **6**, 28441. (doi:10.1038/srep28441)
33. Schnitzer O. 2015 Singular perturbations approach to localized surface-plasmon resonance: nearly touching metal nanospheres. *Phys. Rev. B* **92**, 235428. (doi:10.1103/PhysRevB.92.235428)
34. Schnitzer O, Giannini V, Craster RV, Maier SA. 2016 Asymptotics of surface-plasmon redshift saturation at subnanometric separations. *Phys. Rev. B* **93**, 041409. (doi:10.1103/PhysRevB.93.041409)

35. Hinch EJ. 1991 *Perturbation methods*. Cambridge, UK: Cambridge University Press.
36. Jackson JD. 1999 *Classical electrodynamics*. New York, NY: Wiley.
37. Ruppin R. 1973 Optical properties of a plasma sphere. *Phys. Rev. Lett.* **31**, 1434–1437. (doi:10.1103/PhysRevLett.31.1434)
38. Raza S, Kadkhodazadeh S, Christensen T, Di Vece M, Wubs M, Mortensen NA, Stenger N. 2015 Multipole plasmons and their disappearance in few-nanometre silver nanoparticles. *Nat. Commun.* **6**, 8788. (doi:10.1038/ncomms9788)
39. Cox RG. 1997 Electroviscous forces on a charged particle suspended in a flowing liquid. *J. Fluid Mech.* **338**, 1–34. (doi:10.1017/S0022112097004862)
40. Link S, El-Sayed MA. 1999 Spectral properties and relaxation dynamics of surface plasmon electronic oscillations in gold and silver nanodots and nanorods. *J. Phys. Chem. B* **103**, 8410–8426. (doi:10.1021/jp9917648)
41. Vorobev PE. 2010 Electric field enhancement between two parallel cylinders due to plasmonic resonance. *J. Exp. Theor. Phys.* **110**, 193–198. (doi:10.1134/S1063776110020020)
42. Abramowitz M, Stegun IA. 1972 *Handbook of mathematical functions*. New York, NY: Dover.
43. Jeffrey DJ, Van Dyke M. 1978 The temperature field or electric potential around two almost touching spheres. *IMA J. Appl. Math.* **22**, 337–351. (doi:10.1093/imamat/22.3.337)
44. Hohenester U, Krenn J. 2005 Surface plasmon resonances of single and coupled metallic nanoparticles: a boundary integral method approach. *Phys. Rev. B* **72**, 195429. (doi:10.1103/PhysRevB.72.195429)
45. Hohenester U, Trügler A. 2012 Mnpbem–a matlab toolbox for the simulation of plasmonic nanoparticles. *Comput. Phys. Commun.* **183**, 370–381. (doi:10.1016/j.cpc.2011.09.009)